

**Layer-by-layer Coatings for Phase Change  
Materials: Efficient Thermal Energy Storage Using  
Well-tailored Core-shell Structures**

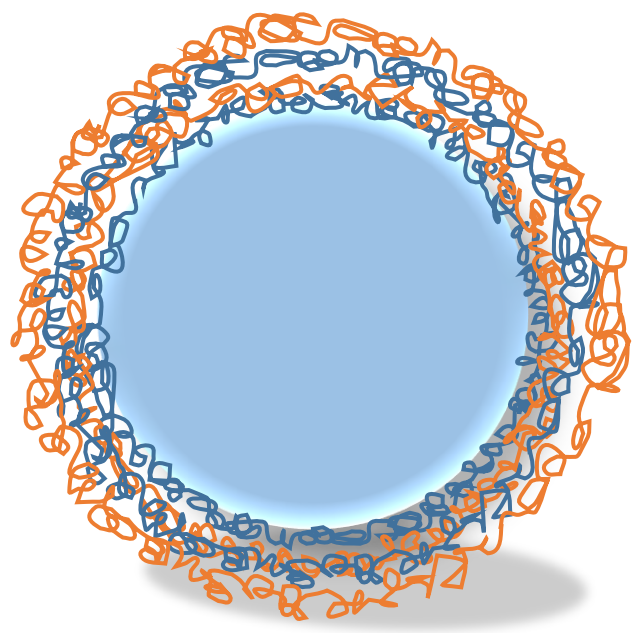


**Steffen Seitz**

A thesis submitted in partial fulfillment of the requirements for the  
degree of Doctor of Philosophy (Engineering)

Division of Materials Science  
Graduate School of Science and Technology  
Nara Institute of Science and Technology

*September 2019*



- Table of Contents -

**Layer-by-layer Coatings for Phase Change  
Materials: Efficient Thermal Energy Storage Using  
Well-tailored Core-shell Structures**

	<i>Page</i>
<b>Chapter 1 – Thermal Energy Storage &amp; Encapsulated PCMs</b>	
<b><i>General Introduction</i></b> .....	<b>1</b>
1.1 Background.....	1
1.2 Thermal Energy Storage.....	1
1.3 Phase Change Materials.....	3
1.4 Encapsulations and the Influence of the Core-Shell Ratio.....	5
1.5 Layer by Layer Self-Assemblies.....	7
1.6 Layer by Layer Encapsulated Phase Change Materials.....	13
1.7 Scope of this thesis .....	14
1.8 References.....	17

## **Chapter 2 – LbL Stereocomplex Coatings for Hydrophilic PCMs**

*Pentaerythritol Particles Covered by Layer-by-Layer Self Assembled Thin Films with*

*Stereocomplex of isotactic Poly(methyl methacrylate) and syndiotactic Poly(methyl*

*methacrylate)*..... **23**

2.1 Introduction..... 23

2.2 Experimental..... 27

2.3 Results and Discussion..... 34

2.4 Conclusion..... 45

2.5 References..... 47

## **Chapter 3 – LbL Polyelectrolyte Coatings for PCMs**

*Self-assembling weak polyelectrolytes for the layer-by-layer encapsulation of paraffin-type*

*phase change material icosane*..... **52**

3.1 Introduction..... 52

3.2 Experimental..... 59

3.3 Results and Discussion..... 65

3.4 Conclusion..... 85

3.5 References..... 87

<b>Concluding Remarks</b> .....	<b>92</b>
<b>List of Publications</b> .....	<b>99</b>
<b>Acknowledgements</b> .....	<b>101</b>

# Chapter 1

## Thermal Energy Storage & Encapsulated PCMs

### *- General Introduction*

#### **1.1 Background**

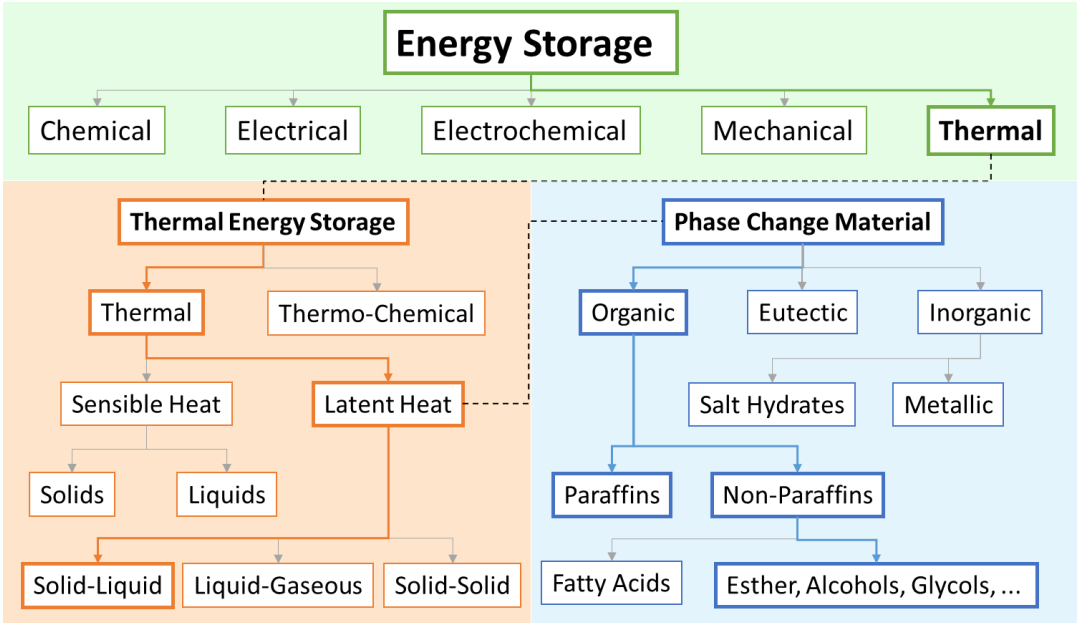
In 2050, human population on earth will reach 9.8 billion.<sup>1</sup> With this massive increase of our planet's population, energy production and supply will become a critical factor for humankind to grow and prosper. Already now, energy topics are providing several challenges. Limited reserves of fossil fuels, concerns over greenhouse gas emissions and drawbacks of renewable energy sources are urging the need to take action and make use of the available energy more efficiently.

#### **1.2 Thermal Energy Storage**

Thermal energy storage (TES) systems are one part of the puzzle to answer to the energy challenge.<sup>2</sup> Identically to a rechargeable battery, TES systems can be charged with energy in the form of heat (= thermal energy). The energy then can be stored, transported if necessary and later on be released. Like this, TES can help to balance energy demands by supplying energy at a variable time scale. It can help to reduce peak demands and overall energy consumption as well as CO<sub>2</sub> emissions and costs while at the same time, it can increase the

efficiency of energy systems and support renewable energies.<sup>3</sup> Industrial waste heat for example is often just released into the environment. If a TES system is used to capture the thermal energy from waste heat streams, the energy can be stored and used in a different process on-site later or it can be stored and transported for off-site use. In both cases, it is not necessary to use fuels to produce new energy, thus costs and emissions are reduced.<sup>4</sup>

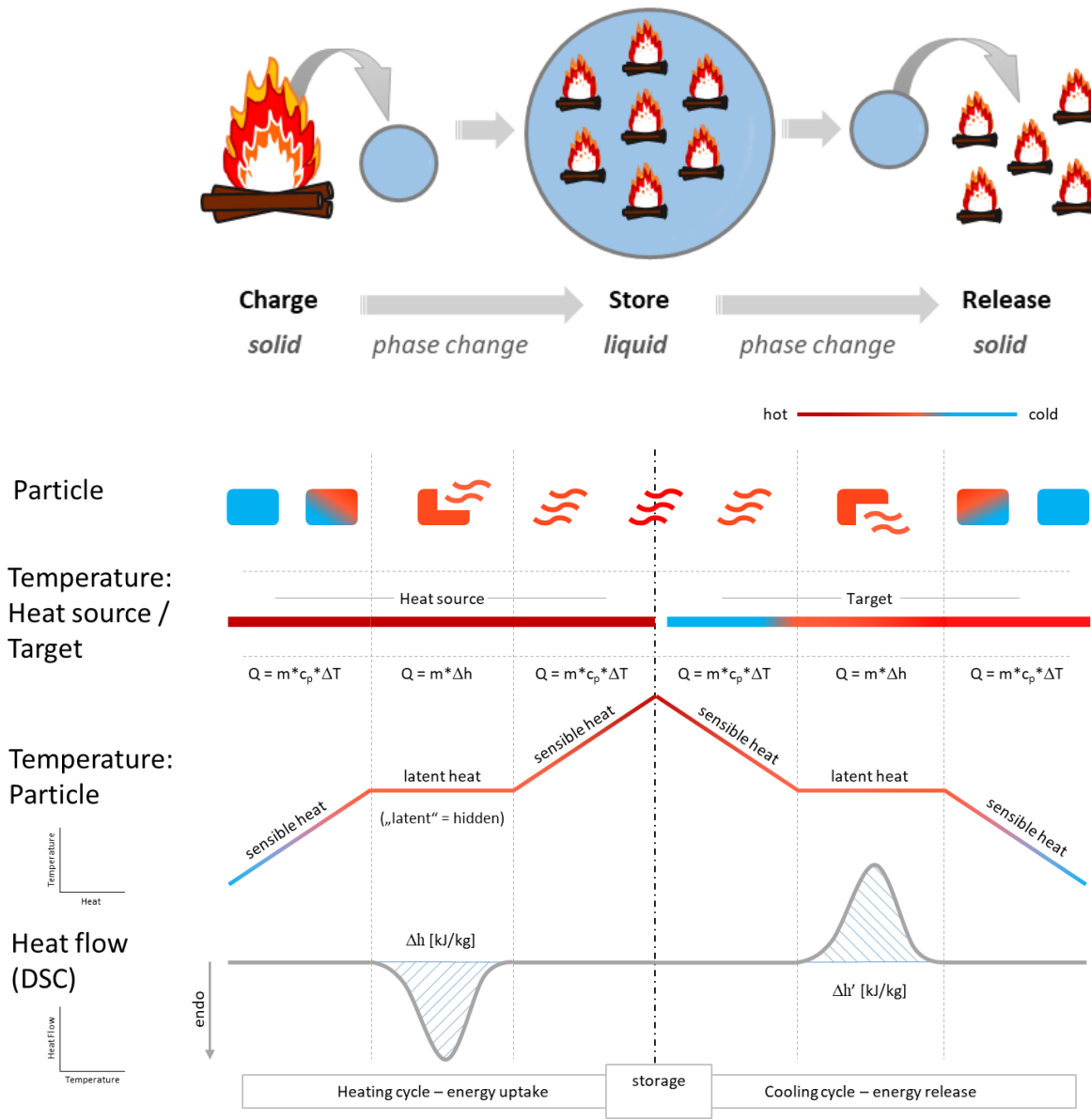
TES can be operated using sensible heat storage, like a hot water storage for example, or using latent heat storage. Latent heat storage is utilizing so-called phase change materials (PCMs) for the storage process. Typical storage periods for sensible heat storage (hot water storage) ranges from several days to seasonal storage with capacities of 10 to 50 kWh/t and estimated costs of 0.1 to 10 €/kWh.<sup>5</sup> For latent heat storage, the range is from several hours to seasonal storage. In that case, storage capacities usually cover 50 to 150 kWh/t at costs of 10 to 50 €/kWh. A general overview of the relations of TES and PCMs is presented in Scheme 1-1.<sup>6,7</sup>



Scheme 1-1: Overview: thermal energy storage and phase change materials.<sup>6,7</sup>

### 1.3 Phase Change Materials

Using latent heat storage systems and therefore PCMs is extremely attractive because of the high storage capacities that can be reached. As the name PCM already implies, the storage process involves a phase change of the storage material. A detailed illustration of the phase change process and the processes taking place during the heat storage are presented in Scheme 1-2.



**Scheme 1-2:** Thermal energy storage using a phase change material. Processes during melting and freezing.



The storage process using a PCM can be described briefly as follows: When heat is supplied from a heat source, the PCM will absorb it as sensible heat first. When the phase transition temperature (here: the melting point) is reached, additional heat does not lead to a further heating of the material, but is entirely used up in the melting process. The temperature of the material at that point remains constant and the absorbed heat is called latent heat. After the phase transition is completed and all the material has melted, further supplied heat will be absorbed as sensible heat again. This process is reversed, when the heat source is removed and the material is allowed to cool. At that time, the latent heat, which was absorbed before, will be released to the environment and can be utilized. Usually, applications for PCMs are designed very carefully and the operation conditions revolve tightly around the phase transition temperatures. This also means that the PCM must be carefully selected according to the desired application. As can be seen from Scheme 1-2, two formulas govern this process,

Sensible heat	$Q = m c_p \Delta T$	(Equation 1-1)
---------------	----------------------	----------------

Latent heat	$Q = m \Delta h$	(Equation 1-2)
-------------	------------------	----------------

where  $Q$  is the heat energy,  $m$  is the mass of the PCM,  $c_p$  is the heat capacity and  $h$  is the phase change enthalpy. It is important to notice that the phase change process is highly influenced by the phase change enthalpy of the PCM. In DSC measurements, the latent heat absorbed or released during the phase change is visualized.

In most cases of using PCMs, there will be a melting and freezing process (solid-liquid

PCMs). However, structural reorganization (solid-solid PCMs) can also be utilized for the energy storage. Due to the large volumetric change, evaporation (liquid-gaseous PCMs) does not play an important role in TES. By reversing the phase change, the stored energy can be released again.




The IRENA technology brief, a report about the development of thermal energy storage systems assessed the market situation for PCMs in 2013.<sup>8</sup> For storage materials in the lower temperature range, usually used for passive cooling, they found a market satisfaction of 75 % and research needs of 25 %. In contrast, high temperature PCMs were evaluated with 0 % market satisfaction and a 100 % need for research. In both cases, the barriers for successful implementation were found among material costs and performance or stability. The main research activities on PCM materials were concerning their encapsulation and material containers.

#### **1.4 Encapsulations and the influence of the core-shell ratio**

Encapsulation can provide numerous advantages to PCMs such as an increased heat transfer area, anti-aggregating properties or a reduced reactivity towards the environment, but also corrosion protecting for the systems in which PCMs are used.<sup>9</sup> However, a major drawback of encapsulation of PCMs is the reduction in storage capacity per gram of materials due to the shell. To prevent a loss of storage capacity, the core-shell ratio play a major role. Table 1-1

shows how a low core-shell ratio can negatively affect the storage capacity of PCMs.

**Table 1-1:** The influence of the core-shell ratio on the storage capacity of a fictional PCM.

Influence of the shell thickness (core-shell ratio)			
Core-shell	100-0	90-10	40-60
Storage capacity, absolute (J/g)	250	225	100
Storage capacity, relative (%)	100	90	40

Many examples in literature show a significant reduction in the storage capacity, when an encapsulation is applied to the material. Table 1-2 compares several encapsulations for an icosane PCM. Icosane is a low temperature PCM with a melting point of 36 °C and a storage capacity of 223.6 J·g<sup>-1</sup>. Manifold publications exist on this highly relevant PCM.

**Table 1-2:** Comparison of different shells for icosane encapsulation.

Shell on C <sub>20</sub> core	T <sub>m</sub> (°C)	H <sub>m</sub> (J/g)	E (%)	Synthesis
C <sub>20</sub> (icosane, C <sub>20</sub> H <sub>42</sub> )	35.7	223.6	/	/
Chitosan/Clay Nanoparticles	35.5	120.5	43.6	Coacervation
SiO <sub>2</sub>	40.5	81.2	33.0	Sol-gel
Poly(methyl methacrylate-co-acrylic acid)	31.7	90.9	32.9	Emulsion polymerization
Ethyl cellulose-co-methyl cellulose	38.0	202.4	90.0	Self assembly
Cu <sub>2</sub> O	38.7	165.3	61.6	Self assembly

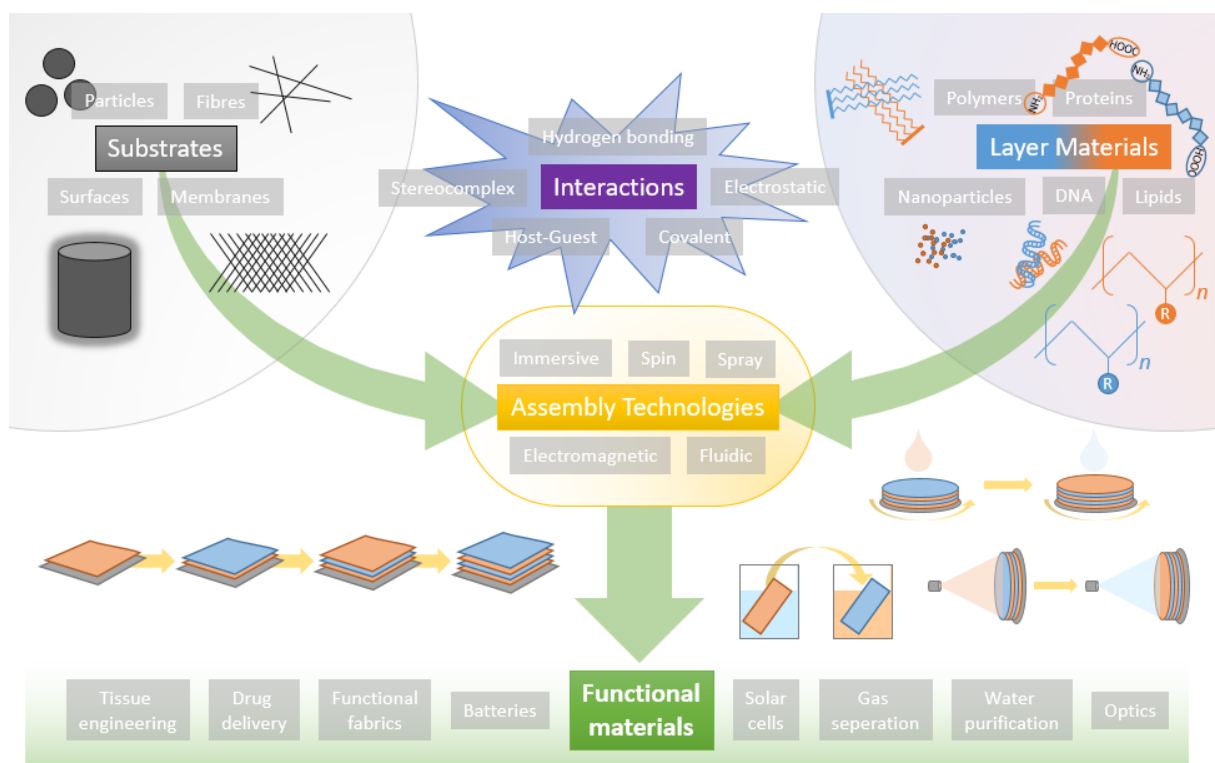
One research group for example used chitosan and clay nanoparticles in a coacervation process as shell material.<sup>10</sup> The resulting material provided a storage capacity of 120.5 J·g<sup>-1</sup>. Another group used a sol-gel process based on SiO<sub>2</sub> to encapsulate icosane. The resulting materials

however could only store  $81.2 \text{ J}\cdot\text{g}^{-1}$ .<sup>11</sup> Moreover, all kinds of polymerization approaches have been applied to form shells on PCMs. An emulsion polymerization preparing poly(methyl methacrylate-co-acrylic acid) as encapsulation resulted in materials able to store  $90.9 \text{ J}\cdot\text{g}^{-1}$ .<sup>12</sup> Finally, self-assemblies are also gaining popularity. The coating of icosane by ethyl cellulose-co-methyl cellulose<sup>13</sup> and shells based on  $\text{Cu}_2\text{O}$ <sup>14</sup> provided materials storing  $202.4 \text{ J}\cdot\text{g}^{-1}$  and  $165.3 \text{ J}\cdot\text{g}^{-1}$  respectively. These examples show how the encapsulation of PCMs can dramatically reduce their storage capacity.

In order to prepare encapsulated PCMs with high storage capacities, a core-shell ratio in the range of 90 % are desirable. Therefore, in this thesis Layer-by-Layer (LbL) self-assemblies were applied for the shell preparation, which are known to produce controllable thickness of the structures at nanometer scale.<sup>15</sup>

### **1.5 Layer-by-Layer Self-assemblies**

In this thesis, Layer-by-Layer (LbL) coatings and suitable core substances are used in order to provide high storage capacity PCMs. Firstly, this chapter is providing an overview of LbL methods in Scheme 1-3.<sup>16</sup>



**Scheme 1-3:** Overview of the principles and fabrication processes of layer-by-layer self-assemblies. Amended from with permission from Richardson et al. *Chem. Rev.*2016, 116(23), 14828-14867. Copyright 2016 American Chemical Society.<sup>16</sup>

Successively, assembly technologies, substrates, interactions among shell materials, and suitable materials themselves will be discussed. Finally, examples of LbL encapsulated PCMs are presented before this chapter is concluded.

Substrates used for LbL self-assemblies can primary be divided into two-dimensional and three-dimensional structures. Secondly, they can be classified as particulate substrates<sup>17,18</sup> or planar substrates<sup>19,20</sup> like fibers, membranes or other surfaces in general (Figure 1-1). The choice

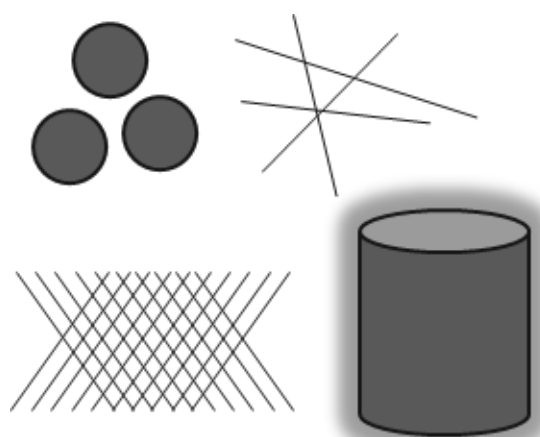


**Figure1-1:** Substrates for LbL self-assemblies include particle, fibers, membranes and surfaces.

of substrates and assembly technology is interdependent. It is necessary to select a suitable coating approach for each substrate. In this aspect, dip coating is highly versatile as it can be used with any kind of substrate mentioned above. Compared to that, planar surfaces but also

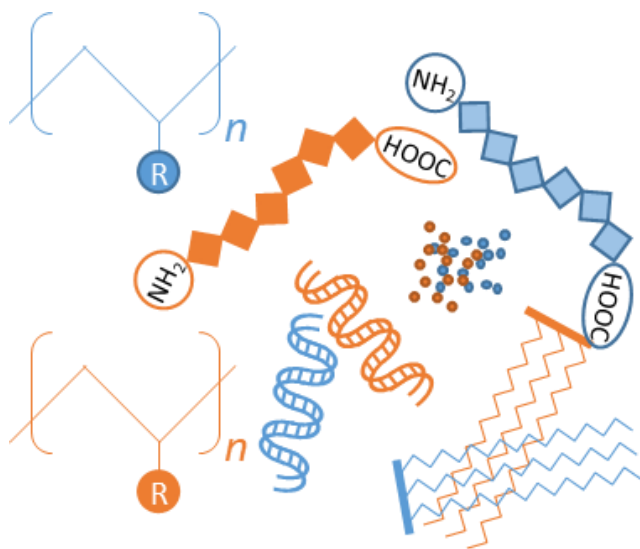
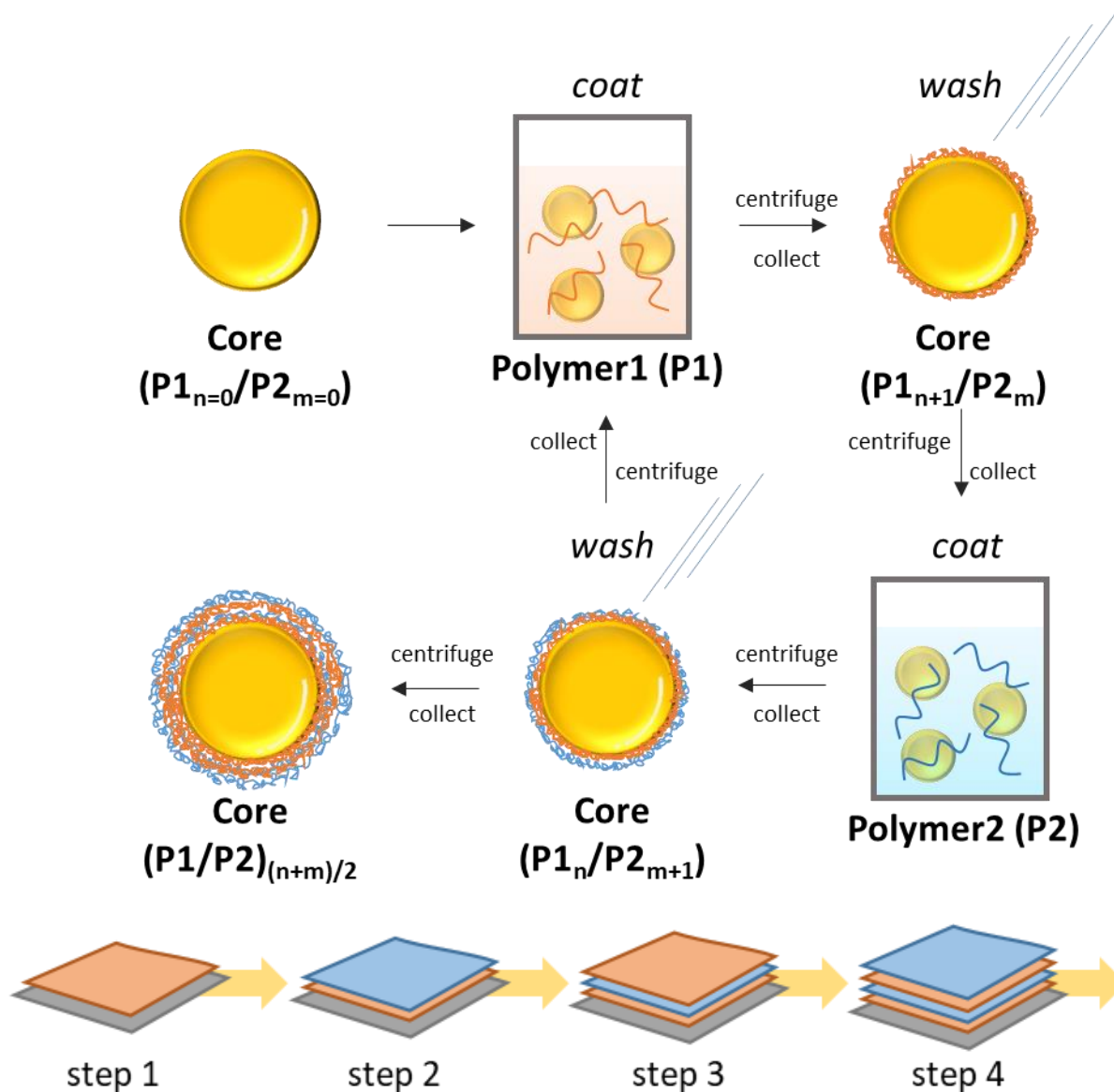


**Figure 1-2:** Materials for LbL self-assemblies include for example polymers, nanoparticles, lipids, proteins and DNA.

particles and simple three-dimensional structures on substrates are suitable for spray coatings whereas this coating approach is ineffective on complex three-dimensional structures such as porous materials for example. In this context,

substrates for spin-coatings usually provide the strictest requirements, as they need to be planar. Layer materials include polymers, nanoparticles, lipids and proteins or DNA for example (Figure 1-2).<sup>21,22</sup> Historically, the LbL concept had been applied to one material class at a time<sup>23</sup>, but recently, more sophisticated approaches emerge that include several material classes.<sup>24,25</sup> Like that, the preparation of highly functional or stimuli responsive materials could be taken to the next level.

The basic principle of the LbL method is the alternating deposition of two different coating materials, which can interact with each other, onto a substrate for a stepwise film growth (Scheme 1-4).



*Scheme 1-4: Stepwise layer growth on a substrate.*

Scheme 1-4 displays the application of the LbL method to a particulate substrate using dip coating and two polymer solutions. The designated core particles are primarily treated with the first polymer solution (here via dip coating). Then, after a sufficient adsorption time and a washing step to remove any loosely bound material, the particles are treated with the second polymer solution and are washed again. This process is repeated until the desired number of layers has been build up. It is important to notice that the particles must not dissolve in the

polymer solutions. That means that the solvent used in the process must on the one side be a good solvent for the coating polymers but on the other side it should be a non-solvent for the particles.

A good control over the shell diameter can be achieved as the thickness of the adsorbed top layer is usually self-regulated through intrinsic factors. For example, if layers are built up through the alternating adsorption of polyanions and polycations, charge inversion will occur on the outer layer during the process, preventing excess amount of polyelectrolyte to be attached.<sup>26</sup> To realize this concept, the coating approach can be varied to match the desired purpose and materials. The main coating approaches include dip coating<sup>27</sup>, spray coating<sup>28</sup> and spin coating<sup>29</sup> (Figure 1-3), but other approaches like fluidic or electromagnetic assemblies have also been developed.

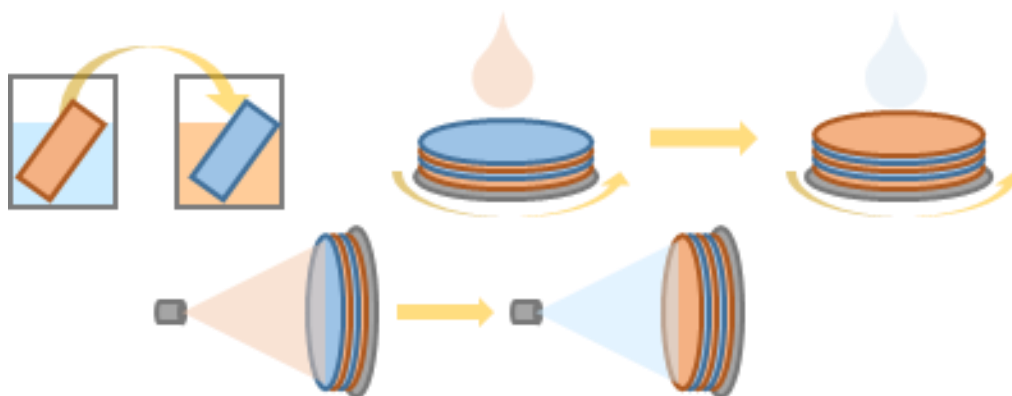


**Figure 1-3:** Major LbL methods - dip coating, spin coating and spray coating.

Major advantages of the LbL technique are a controllable film thickness, usually in the nanometer range, and a very flexible design allowing for a vast variety of layer materials and thus enabling highly adjustable properties for the final materials.



Established by Decher as interaction of polyelectrolytes (polyanions and polycations)<sup>30</sup>, this method was soon extended to other interaction modes like hydrogen bonding<sup>31</sup>, hydrophobic interactions<sup>32</sup>, click-reaction forming covalent bonds<sup>33</sup>, host-guest interactions<sup>34</sup>, biologically specific interactions<sup>35</sup> and stereocomplexation<sup>36</sup>. As each of these molecular interactions comes with their own advantages and disadvantages, careful consideration of the material combination is necessary to produce products with the desired properties.

Covalently bonded layer structures for example can on the one hand be considered highly stable, robust and resistant to harsh environments.<sup>37</sup> On the other hand, these structures are limited in several ways as the layer materials need to be equipped with the proper functional groups. Moreover, after the reaction to form the covalent bonds, side products may remain between the layers as impurities. Generally, this approach can be considered more complex and expensive. In contrast to that, electrostatic interactions are very attractive because of the versatility and brought variety of suitable materials as well as for the good control of the film's structure, composition and properties. This group is by far the most researched. Drawbacks coming along with this approach include the impact that the microenvironment can have on these materials. External stimuli like a change in pH or salt concentration might greatly affect the film stability. The last interaction mode that shall be considered here as an example, is the formation of stereocomplexes. This interaction mode produces highly ordered structures, but is limited to stereoregular polymers.

## 1.6 Layer by Layer encapsulated Phase Change Materials

As described above, LbL self-assemblies produce films in the nanometer order. It is important to notice that the technique used for the encapsulation process as well as the process parameters play a vital role in regards of the deposited amount in each coating step as well as in how the layers arrange. For example, Decher *et al.* assembled poly(styrene sulfonate) poly(allyl amine) films on a fused quartz substrate and measured the increase of the film's thickness in each step by small-angle X-ray scattering.<sup>23</sup> They found an increase of 2.27 nm in each coating step with a linear increase. Another group assembled graphene oxide – poly(ethylene imine) films on a planar substrate and reported a pH dependent increase of the film's thickness. In their experiments, the maximum film growth of 3.45 nm per bilayer was observed at pH 3.5 using atomic force microscopy.<sup>38</sup> In contrast, Sukhorukov *et al.* for example investigated the film growth on particulate poly(styrene sulfonate) latex substrates.<sup>39</sup> They report a stepwise increase of 2 to 2.5 nm per layer during the coating process using poly(diallyl dimethyl ammonium chloride) and poly(styrene sulfonate). These examples sum up the possibilities to produce extremely thin films using LbL self-assemblies and they demonstrate the controllability of the deposited layer thickness through changes in the experimental parameters, here the pH value.

This thesis is built on the assumption that such kind of ultra-thin encapsulation could be highly beneficial for thermal energy storage materials in terms of storage capacity due to a highly suitable core-shell ratio. Surprisingly, there is hardly any report on LbL coated PCMs

for TES to be found in scientific literature. Only one other report that utilizes LbL self-assemblies to prepare encapsulated PCMs was found in a literature research. Some other reports also include LbL self-assemblies into their preparation of encapsulated PCMs, but in these cases, LbL is not the main encapsulation approach. Yi and coworkers used octadecane as the core storage material coated by layered buildup of the strong polyelectrolytes poly(styrene sulfonate) and poly(diallyl dimethyl ammonium chloride).<sup>40</sup> In this context, “strong” refers to the dissociation of the charge bearing groups. In aqueous solution, strong polyelectrolytes will be fully dissociated, whereas weak polyelectrolytes’ dissociation grade of the charge bearing groups is for example dependent on the pH of the solution. Like this, they achieve storage capacities of  $172.8 \text{ J}\cdot\text{g}^{-1}$  at a core-shell ratio of 91.5 % and a melting temperature of  $29.3 \text{ }^\circ\text{C}$ . Pristine octadecane exhibits a storage capacity of  $289.2 \text{ J}\cdot\text{g}^{-1}$  and a melting temperature of  $28.2 \text{ }^\circ\text{C}$ .

## **1.7 Scope of this Thesis**

This thesis includes a detailed description of the LbL method and the application on PCMs for TES.

In Chapter 1, the background of this research thesis is laid out. Briefly, the ideas and concepts are explained and the significance of this research is pointed out in the context of thermal energy storage and phase change materials. Moreover, an explanation about the

importance of choosing the right core-shell combination is given. The core materials must be matched carefully to the polymer solutions, as they must not dissolve therein. For this reason, the following chapters deal with water-soluble and water-insoluble cores separately.

In Chapter 2, the preparation of high temperature storage material pentaerythritol coated by a stereocomplex of stereoregular poly(methyl methacrylate) (PMMA) is described. To provide LbL coatings on water soluble PCMs like sugar alcohols, hydrophobic coating materials have been chosen. Furthermore, in this chapter, a homogenization approach was used for the particle preparation and a suitable solvent system of organic solvents for the particle coating was developed.

In Chapter 3, the target is the fabrication of a low temperature PCM by encapsulation of icosane in oppositely charged polyelectrolytes. Here, a solution for hydrophobic core materials is provided using hydrophilic coatings. An interesting aspect of the combination of weak polyelectrolytes like poly(acrylic acid) and poly(allyl amine) is that they could further be treated in a post assembly process to crosslink the layers and create strong and robust covalent bonds. Compared to chapter 2, the particle preparation method was improved and changed to an emulsion approach, providing more uniform and spherical particles, which are assumed to be coated more easily. Moreover, the solvent system could be changed from organic solvents to the environmentally friendly aqueous system.

In the conclusion section, the prepared materials are compared with similar PCMs from

other research groups to estimate their possible impact in TES. Figure 1-4 presents the contents and relations of each chapter in this thesis.

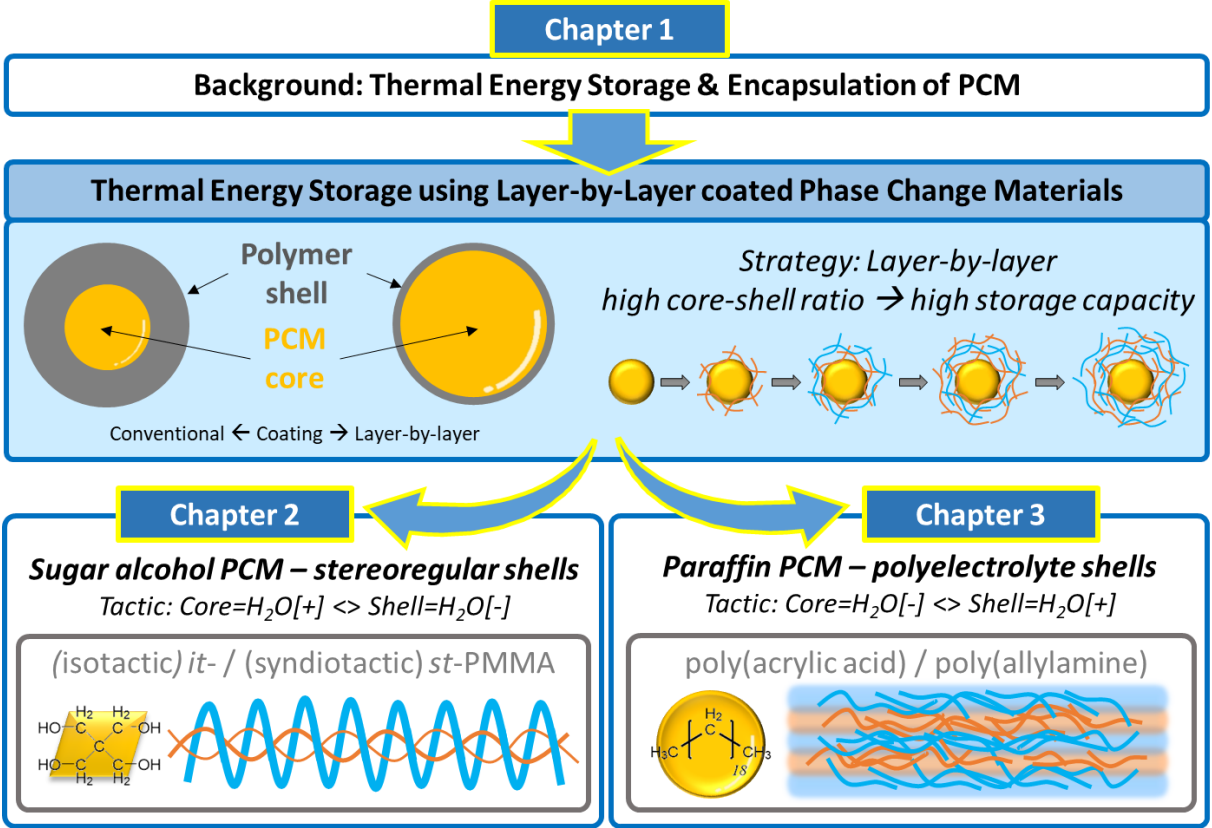


Figure 1-4: Schematic illustration of the contents of this thesis and the relations of each chapter.

It can be seen that the common basis for the materials discussed in the designated chapters consists of LbL coatings to provide high core-shell ratios. By using different material classes, a broad range of applications can be covered. Moreover, also each chapter can be understood by itself, the knowledge of each previous chapter influenced the approaches of the following one and the findings helped to improve the overall outcome of this thesis.

## 1.8 References

- 1 Glenn J. C.; Florescu E. State of the Future. V.19.0. The Millennium Project, 4421 Garrison Street, NW, Washington, D.C. 20016-4055 U.S.A. **2017**.
- 2 Fallahi A.; Guldentops G.; Tao M.; Granados-Focil S.; VanDessel S. Review on solid-solid phase change materials for thermal energy storage: Molecular structure and thermal properties. *Appl. Therm. Eng.* **2017**, *127*, 1427–1441.
- 3 Zhang N.; Yuan Y.; Cao X.; Du, Y.; Zhang Z.; Gui Y. Latent Heat Thermal Energy Storage Systems with Solid–Liquid Phase Change Materials: A Review. *Adv. Eng. Mater.* **2018**, *20*, 1700753.
- 4 Wang W. Mobilized Thermal Energy Storage for Heat Recovery for Distributed Heating. *Dissertation*. Printed by Mälardalen University, Västerås, Sweden, **2010**. ISBN 978-91-86135-98-0.
- 5 Miró L.; Gasia J.; Cabeza L. F. Thermal energy storage (TES) for industrial waste heat (IWH) recovery: A review. *Appl. Energ.* **2016**, *179*, 284-301.
- 6 Sharma A.; Tyagi V. V.; Chen C. R.; Buddhi D. Review on thermal energy storage with phase change materials and applications. *Renew. Sust. Energ. Rev.* **2009**, *13*, 318-345.
- 7 Rathod M. K.; Banerjee J. Thermal stability of phase change materials used in latent heat energy storage systems: A review. *Renew. Sust. Energ. Rev.* **2013**, *18*,

246–258.

- 8 IEA-ETSAP, Irena. Thermal Energy Storage: Technology Brief. **2013**.
- 9 Peng H.; Zhang D.; Ling X.; Li Y.; Wang Y.; Yu Q.; She X.; Li Y.; Ding Y. *n*-Alkanes Phase Change Materials and Their Microencapsulation for Thermal Energy Storage: A Critical Review. *Energ. Fuels*. **2018**, *32*, 7262-7293.
- 10 Genc E.; Sennur A. A. Fabrication of Microencapsulated PCMs with Nanoclay doped Chitosan Shell and Their Application to Cotton Fabric. *Tekst. Konfeksiyon*. **2016**, *26*(2), 180–188.
- 11 He F.; Wang X.; Wu D. Phase-change characteristics and thermal performance of form-stable *n*-alkanes/silica composite phase change materials fabricated by sodium silicate precursor. *Renew. Energ.* **2015**, *74*, 689–698.
- 12 Alkan C.; Aksoy S. A.; Anayurt R. A. Synthesis of poly(methyl methacrylate-co-acrylic acid)/*n*-eicosane microcapsules for thermal comfort in textiles. *Text. Res. J.* **2015**, *85*(19), 2051–2058.
- 13 Phadungphatthanakoon S.; Poompradub S.; Wanichwecharungruang S. P. Increasing the Thermal Storage Capacity of a Phase Change Material by Encapsulation: Preparation and Application in Natural Rubber. *ACS Appl. Mater. Interfaces* **2011**, *3*(9), 3691–3696.
- 14 Gao F.; Wang, X.; Wu, D. Design and fabrication of bifunctional microcapsules for

- solar thermal energy storage and solar photocatalysis by encapsulating paraffin phase change material into cuprous oxide. *Sol. Energy Mater. Sol. C.* **2017**, *168*, 146–164.
- 15 Decher G. Fuzzy Nanoassemblies: Toward Layered Polymeric Multicomposites. *Science.* **1997**, *277*, 1232-1237.
- 16 Richardson J. J.; Cui j.; Björnmalm M.; Braunger J. A.; Ejima H.; Caruso F. Innovation in Layer-by-Layer Assembly. *Chem. Rev.* **2016**, *116*(23), 14828-14867.
- 17 Donath E.; Walther D.; Shilov V.; Knippel E.; Budde A.; Lowack K.; Helm C.; Möhwald H. Nonlinear Hairy Layer Theory of Electrophoretic Fingerprinting Applied to Consecutive Layer by Layer Polyelectrolyte Adsorption onto Charged Polystyrene Latex Particles. *Langmuir.* **1997**, *13*, 5294–5305.
- 18 Hoogeveen N. G.; Cohen Stuart M. A.; Fler G. J.; Böhmer M. R. Formation and stability of multilayers of polyelectrolytes. *Langmuir.* **1996**, *12*, 3675–3681.
- 19 Iler R., Multilayers of colloidal particles. *J. Colloid Interface Sci.* **1966**, *21*, 569–594.
- 20 Lee D.; Rubner M. F.; Cohen R. E. All-nanoparticle thin-film coatings. *Nano Lett.* **2006**, *6*, 2305–2312.
- 21 Richardson J. J.; Cui J.; Björnmalm M.; Braunger J. A.; Ejima H.; Caruso F. Innovation in Layer-by-Layer Assembly. *Chem. Rev.* **2016**, *116*, 14828–14867.



- 22 Guzmána E.; Mateos-Marotoa A.; Ruanob M.; Ortega F.; Rubio R. G. Layer-by-Layer polyelectrolyte assemblies for encapsulation and release of active compounds. *Adv. Coll. Interface Sci.* **2017**, *249*, 290–307.
- 23 Decher G.; Hong J. D.; Schmitt J. Buildup of ultrathin multilayer films by a self-assembly process: III. Consecutively alternating adsorption of anionic and cationic polyelectrolytes on charged surfaces. *Thin Solid Films.* **1992**, *210–211(2)*, 831–835.
- 24 Michel M.; Toniazzo V.; Ruch D.; Ball V. Deposition Mechanisms in Layer-by-Layer or Step-by-Step Deposition Methods: From Elastic and Impermeable Films to Soft Membranes with Ion Exchange Properties. *ISRN Materials Science.* **2012**, Article ID 701695, doi:10.5402/2012/701695
- 25 Borges J.; Mano J. F. Molecular Interactions Driving the Layer-by-Layer Assembly of Multilayers. *Chem. Rev.* **2014**, *114*, 8883–8942.
- 26 Sukhorukov G. B.; Donath E.; Davis S.; Lichtenfeld H.; Caruso F.; Popov V. I.; Möhwald H. Stepwise Polyelectrolyte Assembly on Particle Surfaces: a Novel Approach to Colloid Design. *Polym. Adv. Technol.* **1998**, *9*, 759–767.
- 27 Kolasinska M.; Krastev R.; Gutberlet T.; Warszynski P. Layer-by-Layer Deposition of Polyelectrolytes. Dipping versus Spraying. *Langmuir.* **2009**, *25(2)*, 1224–1232.
- 28 Kharlampieva E.; Kozlovskaya V.; Chan J.; Ankner J. F.; Tsukruk V. V. Spin-

- Assisted Layer-by-Layer Assembly: Variation of Stratification as Studied with Neutron Reflectivity. *Langmuir*. **2009**, 25(24), 14017–14024.
- 29 Chiarelli P. A.; Johal M. S.; Casson J.L.; Roberts J. B.; Robinson J. M.; Wang H. L. Controlled Fabrication of Polyelectrolyte Multilayer Thin Films Using Spin-Assembly. *Adv. Mater.* **2001**, 13, 1167–1171.
- 30 Decher G. Fuzzy Nanoassemblies: Toward Layered Polymeric Multicomposites. *Science*. **1997**, 277, 1232-1237.
- 31 Kharlampieva E.; Kozlovskaya V.; Sukhishvili S. A. Layer-by-Layer Hydrogen-Bonded Polymer Films: From Fundamentals to Applications. *Adv. Mater.* **2009**, 21, 3053–3065.
- 32 Shimazaki Y.; Mitsuishi M.; Ito S.; Yamamoto M.; Inaki Y. Preparation of the nucleoside-containing nanolayered film by the layer-by-layer deposition technique. *Thin Solid Films*. **1998**, 333, 5–8.
- 33 Huang C. J.; Chang F. C. Using Click Chemistry to Fabricate Ultrathin Thermoresponsive Microcapsules through Direct Covalent Layer-by-Layer Assembly. *Macromolecules*. **2009**, 42(14), 5155–5166.
- 34 Zhang J.; Cao W. Self-assembly of small molecules: An approach combining electrostatic self-assembly technology with host-guest chemistry. *New J. Chem.* **2001**, 25, 483–486.

- 35 Müller W.; Ringsdorf H.; Rump E.; Wildburg G.; Zhang X.; Angermaier L.; Knoll W.; Liley M.; Spinke J. Attempts to mimic docking processes of the immune system: recognition-induced formation of protein multilayers. *Science*. **1993**, 262(5140), 1706–1708.
- 36 Ajiro H.; Hinoue T.; Akashi M. Inkjet Approaches Contribute to Facile Isotactic Poly(Methyl)/Syndiotactic Poly(Methyl Methacrylate) Stereocomplex Surface Preparation. *Macromol. Chem. Phys.* **2013**, 214, 1590–1595.
- 37 Kohli P.; Blanchard G. J. Applying Polymer Chemistry to Interfaces: Layer-by-Layer and Spontaneous Growth of Covalently Bound Multilayers. *Langmuir*. **2000**, 16, 4655–4661.
- 38 Zhao L.; Zhang H.; Kim N. H.; Hui D.; Lee J. H.; Li Q.; Sun H.; Li P. Preparation of graphene oxide/polyethyleneimine layer-by-layer assembled film for enhanced hydrogen barrier property. *Composites Part B*. **2016**, 92, 252–258.
- 39 Sukhorukov G. B.; Donath E.; Lichtenfeld H.; Knippel E.; Knippel M.; Budde A.; Möhwald H. Layer-by-Layer Self Assembly of Polyelectrolytes on Colloidal Particles. *Colloids Surf. A*. **1998**, 137, 253–266.
- 40 Yi Q.; Sukhorukov G. B.; Ma J.; Yang X.; Gu Z. Encapsulation of Phase Change Materials Using Layer-by-Layer Assembled Polyelectrolytes. *Int. J. Polym. Sci.* **2015**, Article ID 756237, <http://dx.doi.org/10.1155/2015/756237>

# Chapter 2

## LbL Stereocomplex Coatings for Hydrophilic PCMs

*- Pentaerythritol Particles Covered by Layer-by-Layer Self Assembled Thin Films with Stereocomplex of isotactic Poly(methyl methacrylate) and syndiotactic Poly(methyl methacrylate)*

### 2.1 Introduction

Thermal energy storage can contribute to a responsible use of our limited natural resources and the reduction of greenhouse gas emissions.<sup>1</sup> To store and release excess energy on demand, phase change materials (PCMs) can be used. Hydrogen bonding PCMs often offer large heat storage capacities but may also show disadvantages like sensitivity to environmental influences and leakage.<sup>2</sup> Encapsulation with Layer-by-Layer (LbL) self-assembled thin films<sup>3</sup> is expected to prevent these drawbacks and offer advantages such as an enlarged area of heat transfer.<sup>4</sup>

Encapsulation techniques in general raised considerable interest among the research community as they may provide the PCMs with enlarged heat transfer area, better control of the volume changes and better protection from side reactions with the outside environment.<sup>5</sup> The encapsulation techniques which can be used are varied in a wide range. Hayashi and coworkers for example used interfacial polycondensation reaction using an (W/O) emulsion for

the preparation of erythritol containing microcapsules.<sup>6</sup> Chayasat and coworkers used microsuspension iodine transfer polymerization (ms ITP) to synthesize poly(methyl methacrylate) (PMMA) microcapsules with encapsulated heat storage materials.<sup>7</sup> Other approaches included the fabrication of microencapsulated PCMs using melamine-formaldehyde shells by Zhang and coworkers<sup>8</sup> or the preparation of microcapsules with modified silicon nitride by Yang and coworkers.<sup>9</sup>

On the other hand, there is only one report about the use of the Layer-by-layer (LbL) technique for the encapsulation of heat storage materials as mentioned in chapter 1. Nevertheless, the broad variety of possible applications and variations of this technique<sup>3</sup> made it a suitable candidate for encapsulating PCMs. LbL techniques can provide high controllability of the shell properties, allowing for the design of a shell that is exactly tailored to the needs of the polymer material. The basic principle behind LbL technology originated from a cyclical process of alternating immersion of a substrate into oppositely charged materials' solutions and their absorption onto the substrate and alternately on each other, respectively. Decher was the first to describe the underlying principle in detail<sup>10</sup> and until today, various new applications are created. For example, Grigoriev and coworkers used this technique for the coating of liquid cores.<sup>11</sup> In our group, LbL techniques have been achieved, such as hollow capsules of PMMA stereocomplex<sup>12</sup> and LbL assembly of partially sulfonated isotactic polystyrene with poly(vinylamine).<sup>13</sup> We also emphasized on the use of PMMA to create thin films by template

polymerization.<sup>14</sup> As can be seen from the above mentioned papers, the PMMA is a good candidate for the LbL film, because it forms a stereocomplex which has been thoroughly investigated for example.<sup>15</sup> Many other researchers, who have attempted to characterize the PMMA stereocomplex.<sup>16,17</sup> It is considered that the stereocomplex forming behavior of PMMA and the resulting change in the properties of the stereocomplex (as for example in solubility) are very useful in combination with the LbL process. No other studies referring to the PMMA stereocomplex for coating a PCM for thermal energy storage could be found, but we strongly supposed that *isotactic* (*it*-) PMMA and *syndiotactic* (*st*-) PMMA could well be proper coating materials for PCMs. Briefly, the stereocomplex formation is assumed as follows<sup>15</sup>: In the first step, *it*-PMMA is adsorbed on the substrate by poor solvent driven physisorption. In the second step, *st*-PMMA is adsorbed onto the previously adsorbed *it*-PMMA. In this step, the stereocomplex formation is occurring und spatial rearrangement of the polymer chains (Figure 2-1).

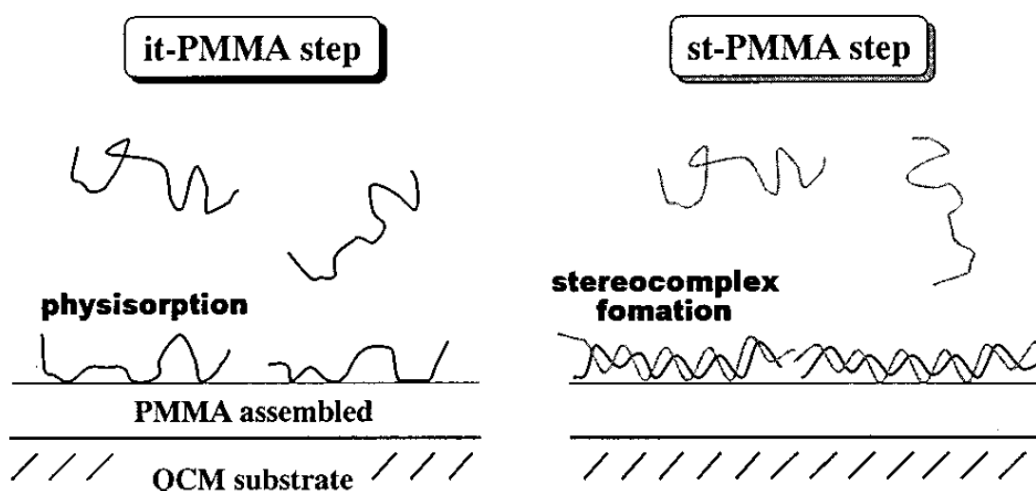


**Figure 2-1:** Illustration of the stereocomplex formation of *it*-PMMA and *st*-PMMA. Reprinted with permission from Serizawa et al. *J. Am. Chem. Soc.* **2000**, 122, 1891-1899. Copyright 2000 American Chemical Society.<sup>15</sup>

In the finally formed stereocomplex, a triple helix structure is formed, where a double stranded helix of it-PMMA is surrounded by a single stranded helix of st-PMMA as presented in Figure 2-2. The exact mechanism of the stereocomplex formation remains subject to the interest of many researchers and is not yet fully understood.

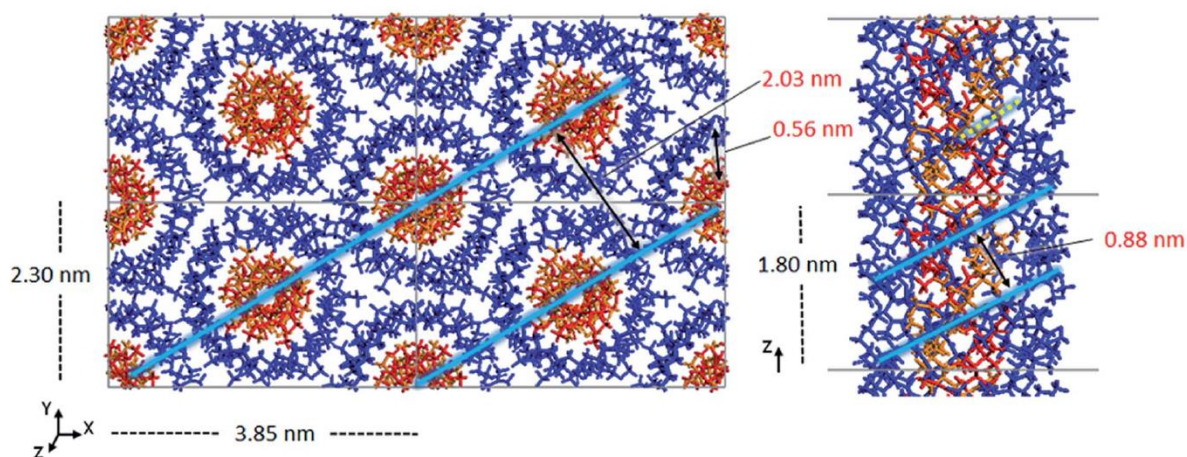


**Figure 2-2:** Computational calculation of the arrangement of the it-PMMA/st-PMMA stereocomplex crystal structure. Licensed under CC BY-NC 3.0; Christofferson et al. *Chem. Sci.*, **2015**, *6*, 1370-1378. - Published by The Royal Society of Chemistry.<sup>18</sup>

As PMMA is not soluble in water, this thesis focused on hydrophilic organic PCMs, which would strongly differ in their solubility from PMMA to perform the LbL process. Exhibiting high phase change enthalpies, low product costs and non-toxic properties, sugar alcohols are one kind of favorable organic phase change materials with suitable melting temperatures for solar process heat and waste heat recovery applications.<sup>19</sup> There are numerous studies using erythritol,<sup>20</sup> mannitol,<sup>21</sup> pentaerythritol<sup>22</sup> or other sugar alcohols as PCM.<sup>23,24</sup>

As Pentaerythritol (PE) exhibits a solid-solid phase change, it was used as a model of a sugar alcohol that cannot leak after its phase change. The phase transition is described as a

rearrangement in the crystal structure of PE. At lower temperatures (25 °C), a body-centered tetragonal structure (Figure 2-3a) determines the internal architecture of the sugar alcohol. In contrast and at higher temperatures (around 189 °C, Figure 2-3b), a more face-centered cubic crystalline structure is adopted. Upon further heating, eventually melting can be achieved when the energy is sufficient to break the supramolecular bonds.<sup>25</sup>

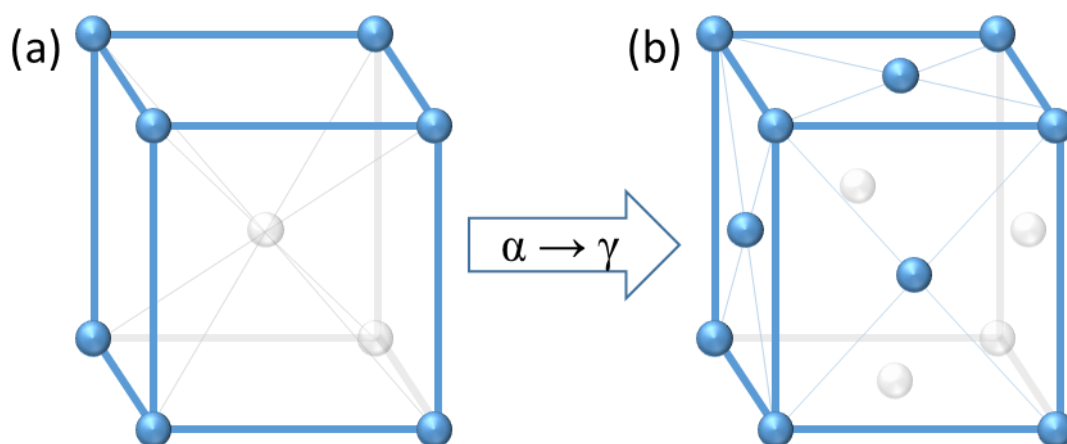


**Figure 2-3:** Schematic explanation of the structural rearrangement in the solid-solid phase change material PE.<sup>25</sup>

The aim of this chapter was to show the general feasibility of coating a sugar alcohol PCM by LbL technique, so the exact conditions of the phase change of the PCM played only a minor role. Herein the successful coating of the hydrogen bonding PCM pentaerythritol by stereocomplex of *it*-PMMA and *st*-PMMA via LbL process is reported.

## 2.2 Experimental

### 2.2.1 Reagents

Pentaerythritol (>98.0 %) was purchased from TCI, Japan and was used without further



purification. *it*-PMMA ( $M_n = 10,000$ , PDI = 1.31) and *st*-PMMA ( $M_n = 20,000$ , PDI = 1.2) (Figure 2-4) were synthesized in earlier experiments. H<sub>2</sub>SO<sub>4</sub> (98 %, Wako, Japan) and hydrogen peroxide (30 %, Wako, Japan) were used to prepare piranha solution (H<sub>2</sub>SO<sub>4</sub>/ hydrogen peroxide, 3/1, v/v) for the cleaning of the quartz crystal microbalances.

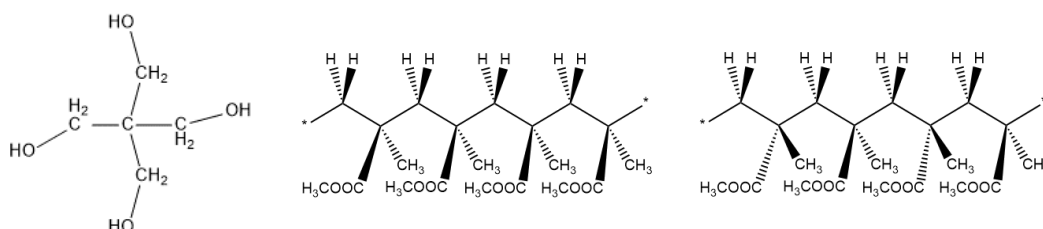


**Figure 2-4:** Chemical structures of pentaerythritol (PE, left), isotactic (*it*-)PMMA (middle) and syndiotactic (*st*-)PMMA (right).

### 2.2.2 Determination of the experimental conditions

Several preliminary experiments were performed to determine the suitable experimental conditions. First, the solvent system was adjusted. Acetonitrile is a theta-solvent for PMMA. Compared with other pure solvents like acetone and DMF, the mass adsorbed on a substrate from PMMA solutions in acetonitrile was up to four times higher in QCM experiments, corresponding to frequency shifts of 0 Hz for adsorption from DMF solutions, 100 Hz for acetone solutions and 400 Hz for acetonitrile solutions after 20 coating steps.<sup>15</sup> However, a mixed solvent system of acetonitrile and water was able to reduce the solubility of PMMA further and deposit even larger amounts on the substrate (corresponding to a frequency shift of 1200 Hz, see Figure 2-6 in section 2.3 for details). In spite of these promising properties,

acetonitrile/water cannot be used as a solvent system as the core material used in this section is highly water-soluble. Instead, another solvent system comprised of hexane/acetonitrile (9:1 v/v) was applied to ensure that the PE particles would not dissolve during the process. An acetone/hexane system was also tested but dismissed because of the PMMA solubility and the expected higher adsorption from hexane/acetonitrile solutions. The stability of the core material was determined in every case through solubility tests of PE in the corresponding solvent systems.

In a second step, the particle preparation approach in the determined hexane/acetonitrile solvent was developed. During the process, the concentration of PMMA was held constant at  $1.7 \text{ mg ml}^{-1}$ , but the particle amount was optimized from 300 mg to 500 mg and the volume of the solution was adjusted to 40 ml to achieve a reasonable dispersion of the particles. The particles were then prepared by homogenization under the above-mentioned conditions (homogenization conditions are laid out under 2.2.3 Apparatus section). A drawback of this approach consists in the obtained particle shape, which cannot be considered spherical but which will resemble a more crystal like structure. Nevertheless, the homogenization approach was chosen because of its simplicity and easy scalability. Moreover, the dip coating approach used herein allows for a complete immersion of the PE particles in the PMMA solutions enabling the polymers to reach and adsorb anywhere on the particle surface. Particle preparation via recrystallization was also considered a suitable approach but was dismissed as it involves

larger amounts of organic solvents and therefore is less environmentally friendly.

### **2.2.3 Apparatus**

Quartz Crystal Microbalances (QCM) (parent frequency 9 MHz, USI, Japan) were thoroughly cleaned with piranha solution right before using in the QCM process and frequency shifts were measured by Frequency Counter (53131A, Agilent, USA) in between each coating step. FT-IR (IR Affinity-1S, Shimadzu, Japan) was used to record FT-IR spectra in a wavenumber range between 400 and 4000  $\text{cm}^{-1}$ . All spectra were measured with a resolution of 4  $\text{cm}^{-1}$  at room temperature. Pictures taken by SEM (SU6600, Hitachi, Japan) were evaluated at different resolutions from 10 to 500 micrometers at magnifications of 220 and 3000 respectively under an acceleration voltage of 1 kV. A homogenizer (AS ONE, AHG-160A, Japan) was used to prepare homogeneous PE particles for both the QCM and the particle coating experiments. The device was used at 60 % of its top rotational-speed for 5 min to homogenize PE particles in acetonitrile/hexane (9/1, v/v). A rotator (Rotator RT-5, TAITEC, Japan) was used during the particle coating to keep the particles suspended in the solution.

### **2.2.4 QCM measurements**

The general experimental procedure of LbL assembly on PCM substrate with QCM has been achieved as described elsewhere.<sup>15</sup> The typical procedure is as follow: 1.7 mg/mL of *it*-PMMA or *st*-PMMA solutions in acetonitrile/hexane (9/1, v/v) were prepared. The 30 mg/mL

of PE solution in deionized water was also prepared in order to coat the QCM substrate.

The PCM process started with cleaning the QCM with piranha solution (one to three drops on each gold contact for 5 min, followed by rinsing with deionized water for 1 min) and preparing the PCM solution as well as the *it*-PMMA and *st*-PMMA solutions. This was followed by measuring the frequency of the cleaned QCM plate using the frequency counter. Then, both sides of the QCM were coated with PE by dipping into the solution. The QCM was kept submerged for 5 min. This was followed by washing the QCM using three drops of the same solvent used for the polymers on each side of the QCM plate. Finally, drying was done in a nitrogen gas flow. Then frequency of the QCM plate was measured again. The so performed preparation was followed by dipping the QCM into *it*-PMMA solution for 5 min to form the first layer. Subsequently the QCM plate was carefully rinsed with three drops of the solvent used for the polymers and dried in a nitrogen gas flow before the frequency of the QCM plate was measured again using the frequency counter. Then the second layer was formed by dipping the QCM into *st*-PMMA solution for 5 min, rinsing the QCM plate carefully with three drops of the solvent used for the polymers, and drying it in a nitrogen gas flow. Measuring the frequency of the QCM plate using the frequency counter was the last step to close one so called cycle. Repeating actions from dipping into *it*-PMMA solution to this last step was supposed to result in the desired amount of layers on the PE substrate attached to the QCM.

After the coating process and measuring the frequency shifts, the QCM was measured

by FT-IR and the frequency shifts were converted to mass attached to the QCM using Sauerbrey's equation.

### 2.2.5 Particle coating

The general experimental procedure of LbL assembly on PCM particles has been also achieved as described in the previous work.<sup>26</sup> The typical procedure is as follow: *it*-PMMA and *st*-PMMA solutions at 1.7 mg/mL in acetonitrile/hexane (9/1, v/v) were similarly prepared. The PE was insoluble in acetonitrile/hexane (9/1, v/v), however, 8 mg of PE was suspended in 1 ml acetonitrile/hexane (9/1, v/v). Then, PE particles were homogenized before the coating process by homogenizer at 60 % of the top tip speed for 5 min. Centrifugation was carried out at 10000 rpm, for 5 min at 25 °C. A schematic illustration of the coating process is given in Figure 2-5.

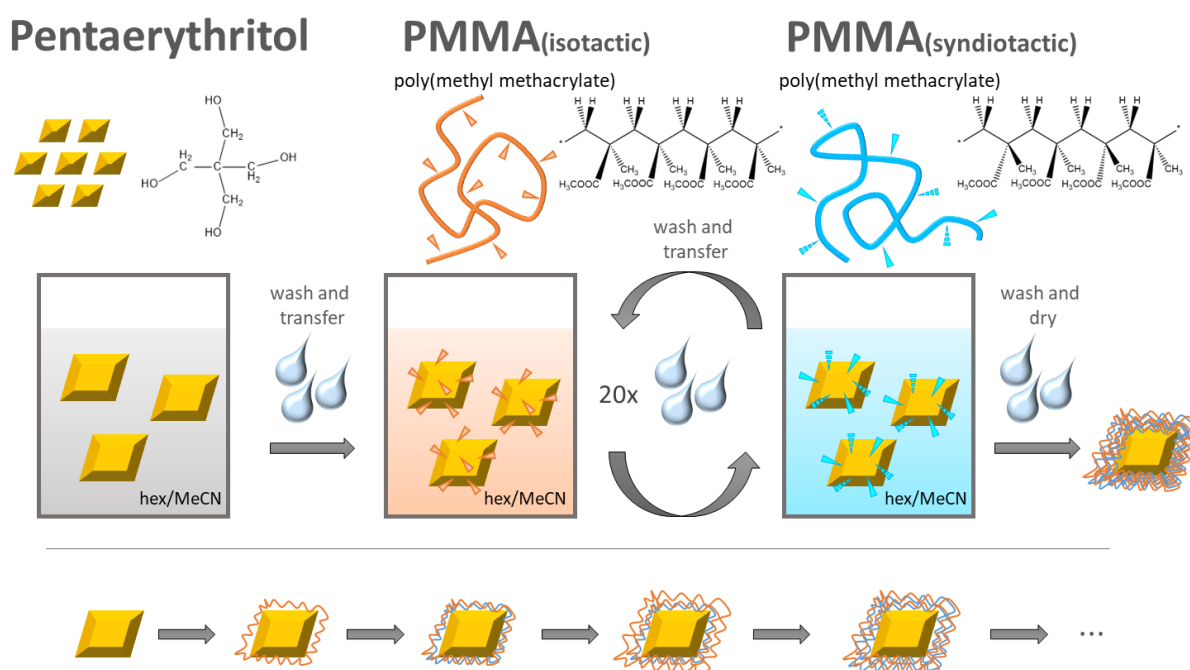


**Figure 2-5:** Schematic illustration of the coating process and the stepwise film growth of PE particles using isotactic and syndiotactic PMMA.

In the first step, *it*-PMMA solution was added to the PE particles. This was followed by rotating the resulting suspension for 5 min by rotator (max speed, 0 ° inclination) to avoid aggregation and improve contact between particles and polymer solution. After that, the suspension was centrifuged and the supernatant polymer solution was removed and collected for further use. A washing solution was added to the particles and slightly shaking the tube was supposed to remove residues of the polymer solution. This step was followed by centrifugation and the removal of the supernatant washing solution. Then, *st*-PMMA solution was added to the particles and rotated again for 5 min under the above-mentioned conditions. The particles were separated from the solution by centrifugation and the supernatant *st*-PMMA solution was collected for further use. Remaining polymer solution again was removed by the use of a washing solution under slightly shaking of the tube. Centrifugation and removal of the supernatant washing solution was the last step of this process. The actions beginning from adding *it*-PMMA solution to the particles until the last step described above were called one cycle resulting in one layer of *it*-PMMA and one layer of *st*-PMMA on the PE particle. By repeating this process, well-defined number of layers can be added.

After the last coating cycle, particles were vacuum dried and observed by SEM. A part of the particles was furthermore washed by water/methanol (1/1, v/v) to remove the PE cores from the particles to observe only the shell material in the SEM. Additionally, the resulting particles from the coating process were measured by FT-IR.

## 2.3 Results and Discussion

In order to demonstrate the feasibility and to implement a model system for the LbL coating of PE initially, a QCM system was used. The basic process and data of coating the PE substrate on the QCM can be seen in Figure 2-6a and Figure 2-6b.

By monitoring the stepwise frequency shift of the QCM after each deposition step of *it*-PMMA and *st*-PMMA, according masses attached to the QCM were calculated using Sauerbrey's equation (Equation 2-1).<sup>27</sup> By doing so, it was possible to show that the *it* PMMA/*st* PMMA stereocomplex can form on a substrate like PE to cover it. This was also confirmed by FT-IR.

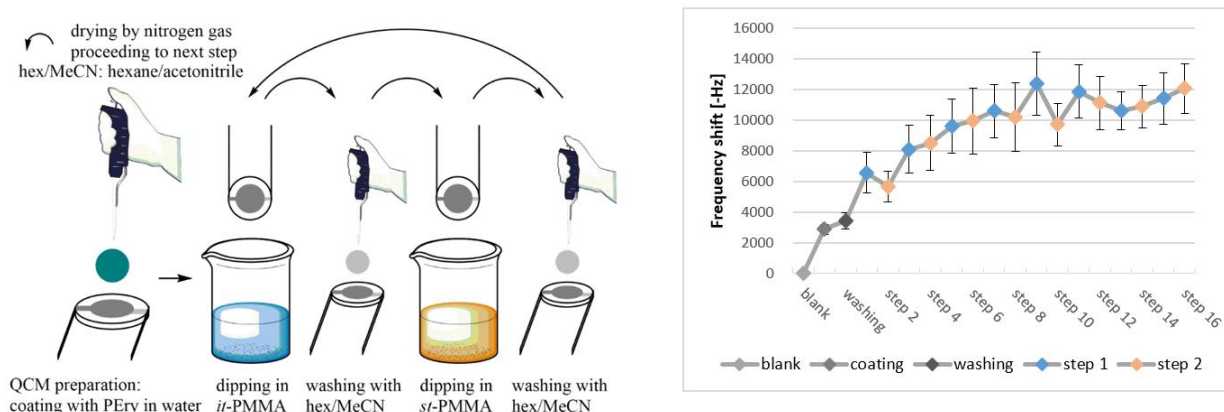


**Figure 2-6.** Schematic image of layer-by-layer assembled process on the QCM substrate (a) and typical analysis of *it*-PMMA/*st*-PMMA on pentaerythritol using QCM substrate. Square = PE, circle = *it*-PMMA, triangle = *st*-PMMA (b).

For the QCM experiments, added masses in each deposition step of *it*-PMMA and *st*-PMMA were calculated from the frequency shifts measured using Sauerbrey's equation,

$$\Delta f = -\frac{2f_0^2}{A\sqrt{\rho_q\mu_q}}\Delta m \quad (\text{Equation 2-1})$$

where  $\Delta f$  is the frequency shift,  $\Delta m$  is the change in mass attached to the QCM,  $A$  is the piezoelectric active area ( $0.159 \text{ cm}^2$ ),  $\rho_q$  is the density ( $2.650 \text{ g cm}^{-3}$ ),  $\mu_q$  is the shear modulus ( $2.94 \times 10^{11} \text{ g cm}^{-1} \text{ s}^{-2}$ ) of the AT-cut quartz crystal and  $f_0$  is its fundamental frequency.

By alternately immersing the QCM into *it*-PMMA and *st*-PMMA solutions respectively, a stepwise LbL assembly of *it*-PMMA and *st*-PMMA to form a stereocomplex on the substrate was expected.

The washing step was conducted by the same solvent being used to make the polymer solution. The good and poor solvent differentiation is important at this point. Solvents used in the process must be able to dissolve the polymer materials (good solvent for polymers allowing for the LbL coating). At the same time, these solvents may not dissolve the PCM layer on the QCM (poor solvent for the PCM). Acetonitrile is known as a theta solvent for PMMA, which is important to mention for the LbL process as well, as it allows for easy polymer-polymer interactions.<sup>28</sup> In a previous report, it was also stated, that the absorbed polymers are stabilized after absorption by polymeric interactions.<sup>15</sup> Figure 2-6b presents the frequency shifts measured in each deposition step ( $n = 5$ ).

Steady increase of the film thickness (from  $\Delta f = -6,567 \text{ Hz}$  at the first *it*-PMMA step to  $\Delta f_{\text{total}} = -12,005 \text{ Hz}$  after the last *st*-PMMA step) can be derived from the graph. The steady



increase in the frequency shift in the adsorption steps strongly implies the attachment of *it*-PMMA and *st*-PMMA onto the PE substrate on the QCM plate. The noticeable aberration at step 11 can be explained by some excess attachment from the solution.

In general, the frequency shifts must be considered very large. The total mass of *it*-PMMA and *st*-PMMA absorbed onto the QCM is calculated to an average of 7474 ng. In a rough calculation, this can be converted to a height of the polymeric coating of about 370 nm, when assuming a density of the coating that is equal to that of solid PMMA (1.18 g cm<sup>-3</sup>). A possible explanation for this phenomenon is seen in the coating of the QCM by PE. Former approaches concentrated on coating the plain QCM. In this case, another substrate is underlying on the QCM. Like that, after the application of PE onto the QCM's surface, surface roughness was most likely changed to higher roughness. This may have resulted in an increased surface area allowing for larger amounts of *it*-PMMA and *st*-PMMA to be attached compared to QCM experiments without the PE layer. This enlarged surface area then has to be covered in every step. This can explain why in general the frequency shifts – meaning the masses attached to the QCM – are larger. Furthermore, solvent effects influencing the amount of absorbed material can also be considered, as a solvent mixture of hexane and acetonitrile was used. Serizawa *et al.* have investigated the effect of various organic solvents on the stereocomplex formation of stereoregular PMMA.<sup>15</sup> When they assembled the stereocomplex on a QCM substrate from *it*-PMMA and *st*-PMMA solutions in acetonitrile, acetone and DMF, they found that acetonitrile,

which is known as a theta-solvent for PMMA, shows the poorest solubility for PMMA and therefore is the best solvent for the adsorption on the substrate (Figure 2-7a). Although all of these solvents were known to produce the PMMA stereocomplex when their solutions of *it*-PMMA and *st*-PMMA were mixed, the situation changed upon the introduction of a substrate to be coated. According to this study, the reason for this behavior is the difference in solubility of PMMA in the specific solvents. When they further decreased the solubility of PMMA by the addition of water to the solvents, the frequency shifts on the QCM increased even more dramatically and additional material was adsorbed (Figure 2-7b). Therefore, it was concluded that the relation of solvent and stereocomplex formation is playing an important role in the assembly process where poor solvents and strong interactions with the substrate yield the best adsorption conditions for the PMMA stereocomplex formation.

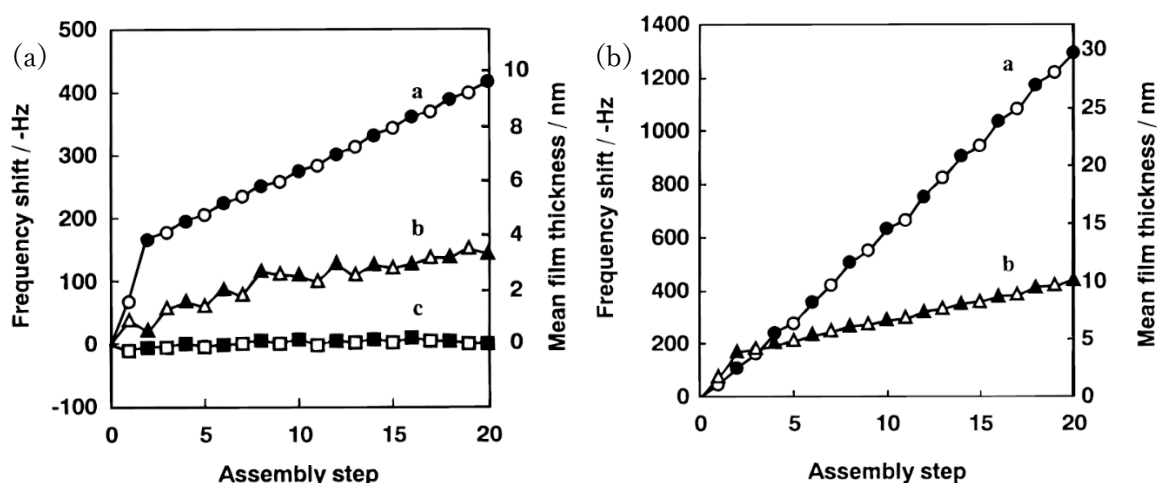


**Figure 2-7:** Left: Stepwise assembly of the PMMA stereocomplex from various solvents on a QCM substrate. *It*-PMMA ( $M_n$  20750) and *st*-PMMA ( $M_n$  22700) were adsorbed from solutions of (a) acetoneitrile, (b) acetone, and (c) DMF at the concentration of  $1.7 \text{ mg ml}^{-1}$ . Right: Stepwise assembly of the PMMA stereocomplex from solutions of (a) acetoneitrile/water, 10/1.5 (v/v) and (b) acetoneitrile under same conditions as mentioned previously. Reprinted with permission from Serizawa et al. *J. Am. Chem. Soc.* **2000**, 122, 1891-1899. Copyright 2000 American Chemical Society.<sup>15</sup>

In general, the stereocomplex formation is very important to the overall process. It enables the polymers to stay attached to the underlying layer through polymeric interaction. Moreover, it is reported to stabilize and insolubilize the absorbed polymer. After calculating the sum of frequency shifts in *it*-PMMA steps and *st*-PMMA steps individually, a 1:1 ratio was found which also was reported for the stereocomplex formation of *it*-PMMA and *st*-PMMA before.<sup>14,17,29</sup>

Thus, the stereocomplex formation can be estimated from the absorbed masses calculated from the frequency shifts of the QCM, but also from the FT-IR/ATR spectra (Figure 2-8).

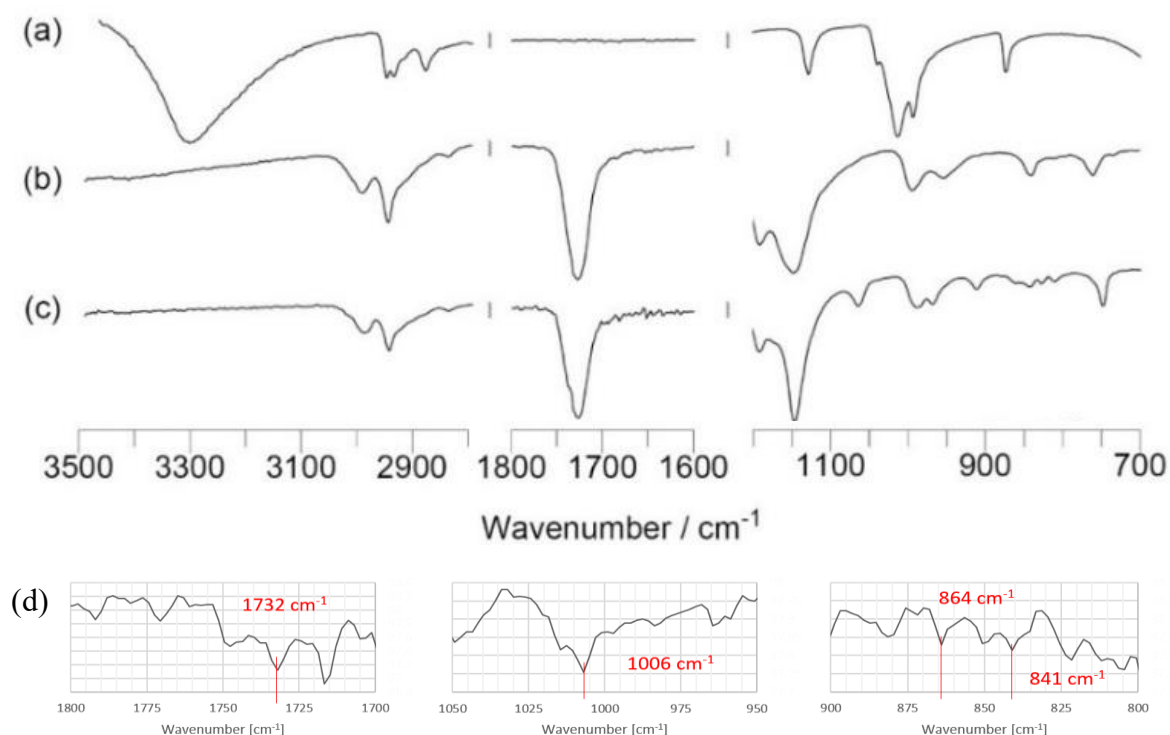


**Figure 2-8:** FT-IR/ATR spectra of PE (a), *it*-PMMA (b), *st*-PMMA (c) and *it*-PMMA/*st*-PMMA LbL assembled PE particles (d).

The specific peaks for the identification of *it*-PMMA, *st*-PMMA, and the stereocomplex

formation were found at about  $1730\text{ cm}^{-1}$  (C=O stretching) and  $842\text{ cm}^{-1}$  ( $\text{CH}_2$ ) and  $862\text{ cm}^{-1}$  ( $\text{CH}_2\text{-}\cdots\text{-CH}_2$ ; stereocomplex).<sup>30</sup> PE could be identified according to the specific peaks at  $1000\text{ cm}^{-1}$  and  $3300\text{ cm}^{-1}$ , which were determined by measurements of pure PE (Figure 2-8a). FT-IR spectra of *it*-PMMA (Figure 2-8b) and *st*-PMMA (Figure 2-8c) showed -C=O stretching at  $1730\text{ cm}^{-1}$ . As mentioned above, LbL thin films of stereoregular PMMA have been investigated by QCM before. It is noteworthy to point out again that this approach differs from the previous work in including an additional substrate in form of PE. The first deposition step of PE as well as the following deposition steps of *it*-PMMA and *st*-PMMA rely on the relatively weak physisorption of the materials on the underlying layer by van der Waals forces. Therefore, the procedures of the LbL coating are sensitive compared to the initial experiments by Decher *et al.* using electrostatic interactions.<sup>10</sup> PE deposition on QCM and PE particles were used as the substrates for *it*-PMMA/*st*-PMMA LbL assembly, and their FT-IR/ATR spectra were compared. The peaks at  $1732\text{ cm}^{-1}$ , is assigned to the -C=O double bond in PMMA (Figure 2-8d).

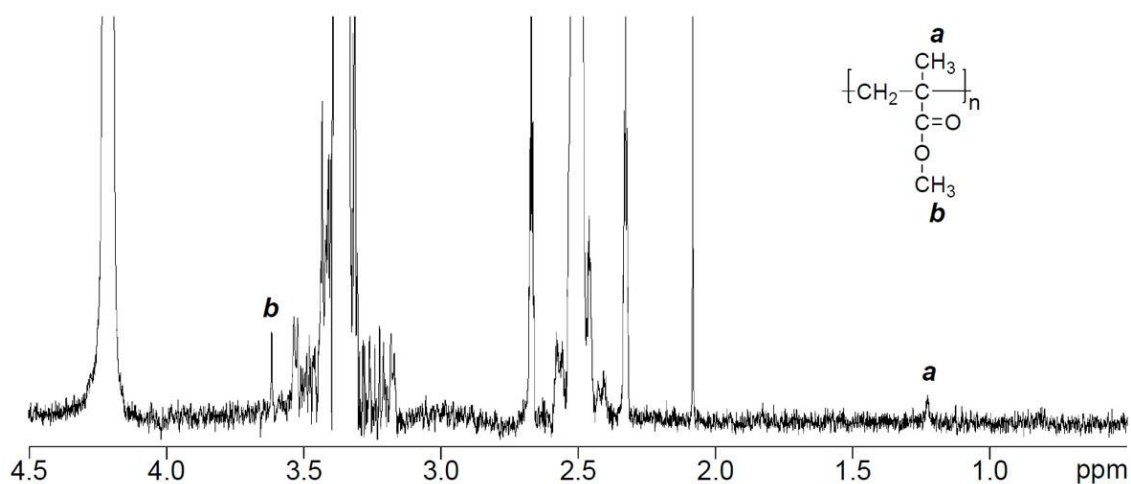


**Figure 2-9:** <sup>1</sup>H NMR spectra of LbL assembled PE particles (in CDCl<sub>3</sub>, r.t., 400 MHz).

The peak at a frequency of 841 cm<sup>-1</sup> assigns the presence of PMMA and the peak at 864 cm<sup>-1</sup> indicates the formation of the stereocomplex. On the other hand, the peak at about 1006 cm<sup>-1</sup> indicates the presence of PE. From this measurement, stereocomplex formation on the PE particle can be assumed on the particles (Figure 2-8d).

The existence of PMMA on PE particles was also confirmed by <sup>1</sup>H NMR spectrum (Figure 2-9). Since most of the volume was occupied by PE, the peak intensity was difficult to observe, however, the PMMA was recognized. The specific peaks at 1.2 ppm for alpha-methyl of *it*-PMMA and 1.05 ppm for that of *st*-PMMA were observed, although the peak intensities were low due to the much smaller amount of polymers compared to PE. Moreover, the peak at 3.6 ppm for methyl ester part of PMMA were confirmed. Further indices for the successful LbL covering of PE can be derived from the comparison of the SEM analysis of particles, which were used in the LbL process, and particles, which did not receive a coating. Figure 2-10 shows several SEM frames in different resolutions.

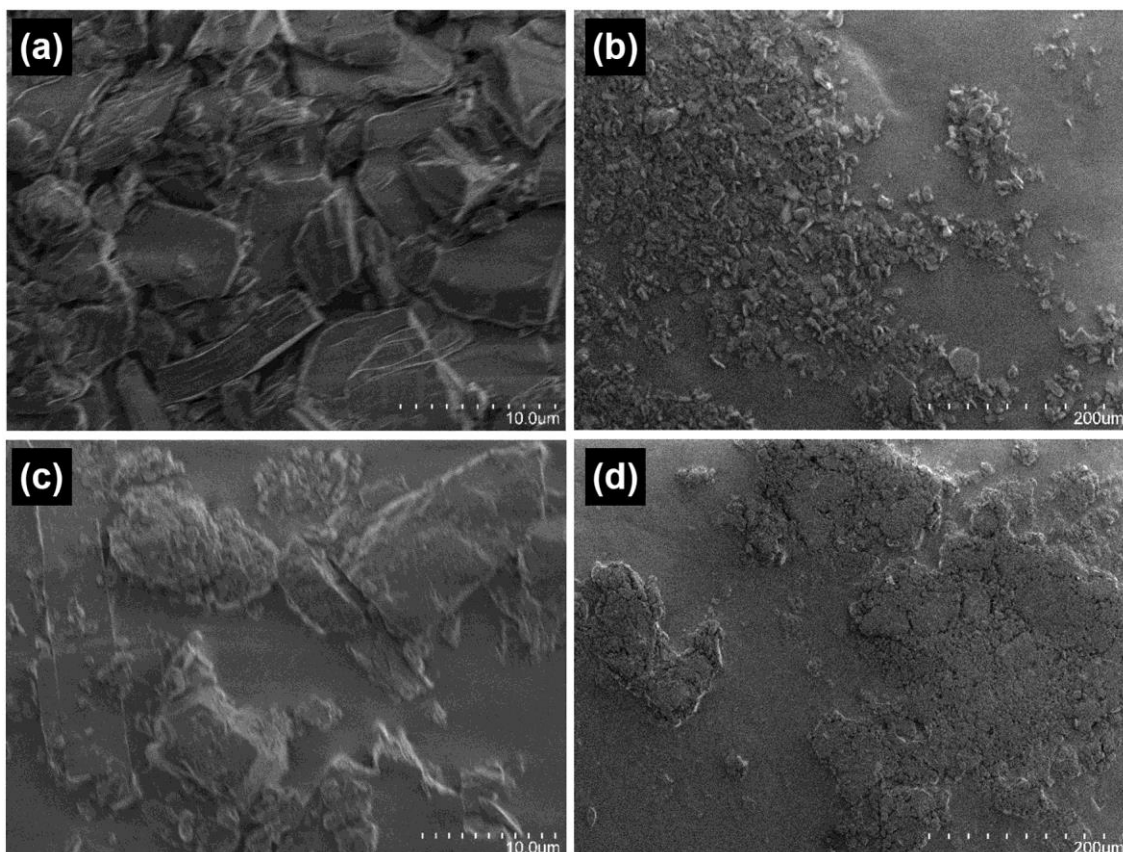
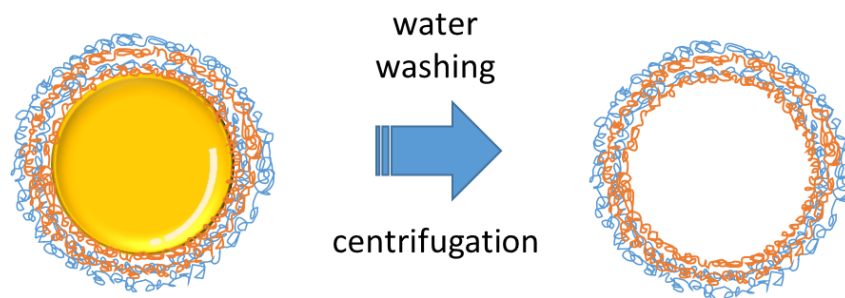


**Figure 2-10:** SEM images of the *it*-PMMA/*st*-PMMA coated particles with high magnification (a) and low magnification (b). SEM images of coated particles after washing out of the pentaerythritol cores with high magnification (c) and low magnification (d).

Figure 2-10a and 2-10b show coated PE, and Figure 2-10c and 2-10d show LbL treated PE particles after 20 cycles and washing with MeOH/water (1/1, v/v) to remove the PE cores. The direct comparison of the uncoated particles to their coated and washed counterparts reveals differences in topology and aggregation behavior. At 3000 times magnification, the uncoated PE particles show loose bulk material with sharply defined edges, whereas the coated particle

residues show massive aggregation and are rather smooth at the edges (Figure 2-10c). As the PE cores are supposed to be removed by the MeOH/water washing step, most of the remaining very small particles are supposed to be *it*-PMMA/*st*-PMMA stereocomplex (Figure 2-10c). Obviously, not all PE could be removed by the washing step at the end of the coating procedure. This may be explained in two ways. On the one hand, some of the particles could just have remained because the volume used to wash was small with 2 ml per washing step. On the other hand, some aggregations could possibly have prevented the washing solution from reaching the particles; hence, not all PE was removed.

Observing the 200 times magnification pictures, the same aspects can be recognized. Here again it can be seen that definitely not all PE particles were removed by the washing steps, as some larger crystals remained. However, a closer look at Figure 2-10d reveals some very small aggregations on the upper left side of the picture. These very small aggregations cannot be found on Figure 2-10b and are therefore assigned PMMA residues. Unfortunately, the pictures do not show some clearly visible capsules. This is due to the fact, that capsules, which formed during the coating process, may eventually be compressed and smothered by the centrifugation forces after the PE cores were removed. This would also explain about the fine and very dense aggregations seen in Figure 2-10c in comparison to the uncoated particles.

In general, the comparison of uncoated, and coated and washed particles shows differences in topology and aggregation behavior. Coated particles were also investigated

without prior washing, but showed no difference in appearance to the uncoated particles used here. This result, together with the FT-IR/ATR, can be interpreted as successful LbL coating of the PE particles.

Finally, the thermal properties of the LbL coated PE particles were demonstrated with DSC and TGA, in order to show the possible of thermal storage application (Figure 2-11).

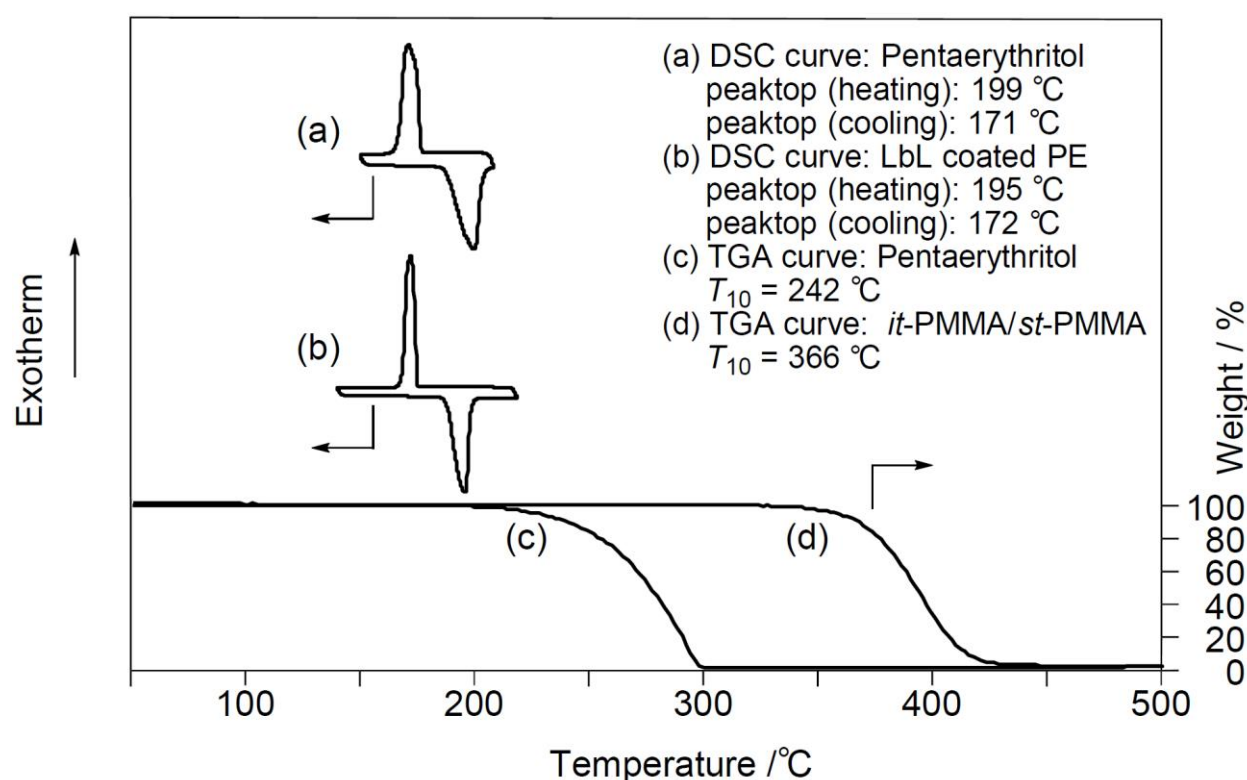


**Figure 2-11:** DSC traces of the *it*-PMMA/*st*-PMMA coated PE particles (a) and PE (b). Data of the second heating is used. The peaks show the solid-solid transition from crystal II to crystal I upon heating and from crystal I to crystal II upon cooling. TGA analysis of PE (c) and the *it*-PMMA/*st*-PMMA (d).

It is known that PE has solid-solid transition property, that shows at around 185 °C from crystal II to crystal I.<sup>31,32</sup> The heating phase transition temperature of PE particle was observed at 199 °C (Figure 5a), which was almost the same as that of *it*-PMMA/*st*-PMMA coated PE particles at 195 °C (Figure 2-11b). The cooling phase transition was observed at 172 °C, which



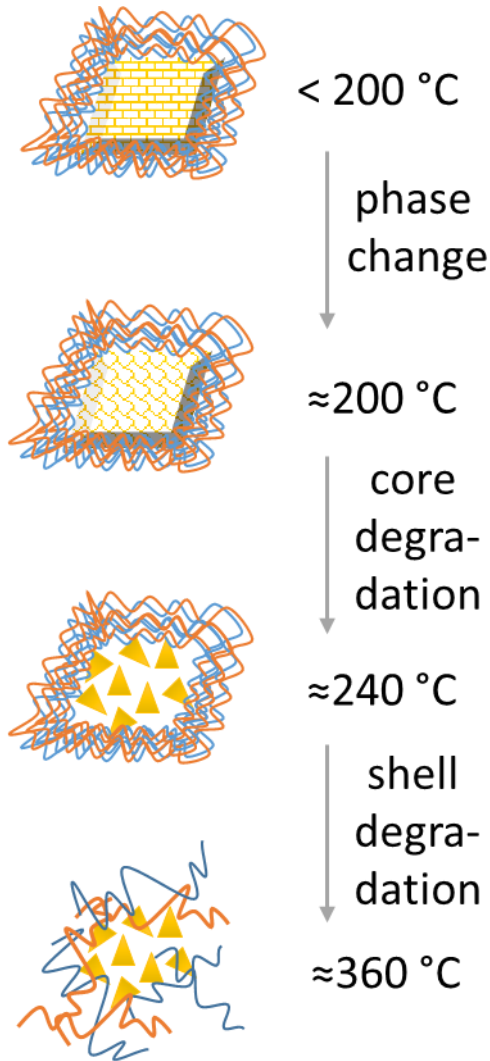


**Figure 2-12:** Schematic illustration of the DSC and TGA results.

is also fairly close to the pure PE particle's transition temperature of 171 °C. The phase change temperatures show good agreement. We conclude that the thin layer of PMMA stereocomplex has no significant influence on the transition temperatures.

When  $T_{10}$  was defined as the temperature at 10% weight loss for thermal decomposition, PE showed  $T_{10}$  at 242 °C (Figure 2-11c), whereas  $T_{10}$  of *it*-PMMA and *st*-PMMA was 366 °C (Figure 2-11d).

The findings from TGA and DSC evaluations have are illustrated in Figure 2-12. It can be seen that the

phase transition at around 200 °C is the first event during the heating process, followed by the

beginning degradation of the core material (around 240 °C) and finally resulting in the degradation of the shell material and the destruction of the particles (around 360 °C). These results suggest that *it*-PMMA/*st*-PMMA could be utilized for coating film for PE particles with the range of phase change temperature. It is noteworthy that the LbL coating for PCM means the stabilization and the surface functionalization. The successful results contribute to the development of functionalization of PCM in various application in the future.

## 2.4 Conclusion

In order to coat PCM by LbL approach, the possibility to cover the hydrogen-bonding compound, PE, was investigated with *it*-PMMA/*st*-PMMA by LbL technique. QCM, topological SEM examinations, and FT-IR measurements were able to detect step-by-step film growth, differences in topologies and the specific peaks of the applied materials. *It*-PMMA/*st*-PMMA stereocomplex formation onto the PE substrate thus was assumed in both cases, QCM and particle coating. Thermal properties of PE and PMMA revealed the stability of the particle for the use of thermal storage of *it*-PMMA/*st*-PMMA coated PE particles. Therefore, the introduction of the *it*-PMMA/*st*-PMMA stereocomplex as a coating film to hydrogen-bonding phase change material PE was achieved. Like this, it was revealed that the LbL coating of water soluble, less stable materials in comparison to usually used silica particles or porous metal substrates is also possible by LbL technique using *it*-PMMA and *st*-PMMA.

As mentioned in the introduction, using water-soluble cores and hydrophobic shell materials was the first core-shell combination to be considered. It can be assumed that this approach is transferable to other water-soluble core PCMs. Contrary to that, water-insoluble PCMs need a different coating and a different solvent that goes along with that. According to that, a suitable approach is presented in the following chapter. Moreover, a weakness in the coating process presented in chapter 2 is the particle preparation process by homogenizer. To improve the particle quality in terms of uniformity and to create spherical particles, chapter 3

will include an emulsion method for the particle preparation.

## 2.5 References

- 1 Sharma A.; Tyagi V. V.; Chen C. R.; Buddhi D. Review on thermal energy storage with phase change materials and applications. *Renew. Sust. Energ. Rev.* **2009**, *13*, 318-345.
- 2 Pielichowska K.; Pielichowski K. Phase change materials for thermal energy storage. *Prog. Mater. Sci.* **2014**, *65*, 67-123.
- 3 Richardson J. J.; Bjoernmalm M.; Caruso F. Multilayer assembly. Technology-driven layer-by-layer assembly of nanofilms. *Science.* **2015**, *348*(6233), aaa2491, DOI: 10.1126/science.aaa2491.
- 4 Al-Shannaq R.; Farid M.; Al-Muhtaseb S.; Kurdi J. Emulsion stability and cross-linking of PMMA microcapsules containing phase change materials. *Sol. Energ. Mater. Sol. C.* **2015**, *132*, 311-318.
- 5 Farid M. M.; Khudhair A. M.; Razack S. A. K.; Al-Hallaj S. A review on phase change energy storage: materials and applications. *Energ. Convers. Manage.* **2004**, *45*, 1597-1615.
- 6 Hayashi Y.; Fuchigami K.; Taguchi Y.; Tanaka M. Preparation of microcapsules containing erythritol with interfacial polycondensation reaction by using the (w/o) emulsion. *J. Encapsul. Adsorp. Sci.* **2014**, *4*, 132-141.
- 7 Chaiyasat P.; Noppalit S.; Okubo M.; Chaiyasat A. Innovative synthesis of high performance poly(methyl methacrylate) microcapsules with encapsulated heat storage

- material by microsuspension iodine transfer polymerization (ms ITP). *Sol. Energ. Mat. Sol. C.* **2016**, *157*, 996-1003.
- 8 Zhang H.; Wang X. Fabrication and performances of microencapsulated phase change materials based on n-octadecane core and resorcinol-modified melamine–formaldehyde shell. *Colloid. Surf. A.* **2009**, *332*, 129-138.
- 9 Yang Y.; Kuang J.; Wang H.; Song G.; Liu Y.; Tang G. Enhancement in thermal property of phase change microcapsules with modified silicon nitride for solar energy. *Sol. Energ. Mat. Sol. C.* **2016**, *151*, 89-95.
- 10 Decher G. Fuzzy nanoassemblies: toward layered polymeric multicomposites. *Science.* **1997**, *277*, 1232-1237.
- 11 Grigoriev D. O.; Bukreeva T.; Möhwald H.; Shchukin D. G. New Method for Fabrication of Loaded Micro- and Nanocontainers: Emulsion Encapsulation by Polyelectrolyte Layer-by-Layer Deposition on the Liquid Core. *Langmuir.* **2008**, *24*, 999-1004.
- 12 Kida T.; Mouri M.; Akashi M. Fabrication of Hollow Capsules Composed of Poly(methyl methacrylate) Stereocomplex Films. *Angew. Chem. Int. Ed.* **2006**, *45*, 7534-7536.
- 13 Ajiro H.; Beckerle K.; Okuda J.; Akashi M. Layer-by-layer assembly of partially sulfonated isotactic polystyrene with poly(vinylamine). *Langmuir.* **2012**, *28*, 5372-5378.

- 14 Ajiro H.; Kamei D.; Akashi M. Mechanistic Studies on Template Polymerization in Porous Isotactic Poly(methyl methacrylate) Thin Films by Radical Polymerization and Postpolymerization of Methacrylate Derivatives. *Macromolecules*, **2009**, *42*, 3019-3025.
- 15 Serizawa T.; Hamada K.; Kitayama T.; Fujimoto N.; Hatada K.; Akashi M. Stepwise Stereocomplex Assembly of Stereoregular Poly(methyl methacrylate)s on a Substrate. *J. Am. Chem. Soc.* **2000**, *122*, 1891-1899.
- 16 Schomaker E.; Challa G. Complexation of stereoregular poly(methyl methacrylates). 14. The basic structure of the stereocomplex of isotactic and syndiotactic poly(methyl methacrylate). *Macromolecules*. **1989**, *22*, 3337-3341.
- 17 Nishiura T.; Kitayama T.; Hatada K. Intra- and Intermolecular Stereocomplex Formation of Uniform Stereoblock Poly(methyl methacrylate). *Polym. J.* **1996**, *28*, 1021-1023.
- 18 Christofferson A.J.; Yiapanis G.; Ren J.M.; Qiao G.G.; Satoh K.; Kamigaito M.; Yarovsky I. Molecular mapping of poly(methyl methacrylate) super-helix stereocomplexes. *Chem. Sci.*, **2015**, *6*, 1370-1378.
- 19 Solé A.; Neumann H.; Niedermaier S.; Martonell I.; Schossig P. Stability of sugar alcohols as PCM for thermal energy storage. *Sol. Energ. Mat. Sol. C.* **2014**, *126*, 125-134.
- 20 Zhang X.; Chen X.; Han Z.; Xu W. Study on phase change interface for erythritol with nano-copper in spherical container during heat transport. *Int. J. Heat. Mass. Trans.* **2016**,

- 92, 490-496.
- 21 Kumaresan G.; Velraj R.; Iniyan S. Thermal analysis of D-mannitol for use as phase change materials for latent heat storage. *J. Applied. Sci.* **2011**, *16*, 3044-3048.
- 22 Hu P.; Zhao P. P.; Jin Y.; Chen Z. S. Experimental study on solid–solid phase change properties of pentaerythritol (PE)/nano-AlN composite for thermal storage. *Sol. Energ.* **2014**, *102*, 91-97.
- 23 Gunasekaraa S. N.; Pana R.; Chiua J. N.; Martina V. Polyols as Phase Change Materials for Low-grade Excess Heat Storage. *Energy Procedia.* **2014**, *61*, 664-669.
- 24 PalomoDelBarrio E.; Cadoret R.; Daranlot J.; Achchaq F. New sugar alcohols mixtures for long-term thermal energy storage applications at temperatures between 70 °C and 100 °C. *Sol. Energ. Mat. Sol. C.* **2016**, *155*, 454-468.
- 25 Fallahi A.; Guldentops G.; Tao M.; Granados-Focil S.; VanDessel S. Review on solid-solid phase change materials for thermal energy storage: Molecular structure and thermal properties *Appl. Therm. Eng.* **2017**, *127*, 1427–1441.
- 26 Serizawa T.; Hamada K.; Akashi M. Polymerization within a molecular-scale stereoregular template. *Nature.* **2004**, *429*, 52-55.
- 27 Sauerbrey G. Verwendung von Schwingquarzen zur Wägung dünner Schichten und zur Mikrowägung. *Z. Phys.* **1959**, *155*, 206-222.
- 28 Ajiro H.; Hinoue T.; Akashi M. Inkjet Approaches Contribute to Facile Isotactic

- Poly(Methyl)/Syndiotactic Poly(Methyl Methacrylate) Stereocomplex Surface Preparation. *Macromol. Chem. Phys.* **2013**, *214*, 1590-1595.
- 29 Lohmeyer J. H. G. M.; Tan Y. Y.; Lako P.; Challa G. Stereoselective association between isotactic poly(methyl methacrylate) and syndiotactic poly(methacrylic acid). *Polymer*. **1978**, *19*, 1171-1175.
- 30 Mihailov M.; Dirlikov S.; Peeva N.; Georgieva Z. Conformational Structure and Stereocomplex Formation in Poly(methyl methacrylate). *Macromolecules*. **1973**, *6*, 511-513.
- 31 Domalski E. S.; Hearing E. D. Heat Capacities and Entropies of Organic Compounds in the Condensed Phase. Volume III. *J. Phys. Chem. Ref. Data*. **1996**, *25*, 1-525.
- 32 Feng H.; Liu X.; He S.; Wu K.; Zhang, J. Studies on solid–solid phase transitions of polyols by infrared spectroscopy. *Thermochimica Acta*. **2000**, *348*, 175-179.



# Chapter 3

## LbL Polyelectrolyte Coatings for PCMs

*- Self-assembling weak polyelectrolytes for the layer-by-layer encapsulation of paraffin-type phase change material icosane*

### 3.1 Introduction

Significant efforts have been made to encapsulate solid-liquid phase change materials (PCMs) for the use in thermal energy storage.<sup>1,2</sup> Providing major advantages like an increased heat transfer area, the prevention of leakage, a reduced reactivity towards the environment, and increased durability of the PCM core material, numerous encapsulation approaches have emerged to put PCMs to the best of their possibilities.<sup>3</sup> The growing number of specific review papers on the encapsulation of PCMs is proof of the importance of this concept.<sup>1-5</sup> Among others, electrospinning<sup>6</sup>, Pickering emulsion<sup>7</sup>, emulsion polymerization<sup>8</sup>, stirred emulsions<sup>9</sup>, and micro suspension iodine transfer radical polymerization<sup>10</sup> have been exploited to form PCM capsules.

Despite being effective in forming stable shells, these encapsulation approaches come with several drawbacks; for example, they can require advanced preparation methods including mini emulsion polymerization<sup>11</sup> or multistep processes<sup>12</sup>. Another major difficulty is found in achieving high storage capacities, referring to high PCM content in the capsules. Makuta *et al.* for example report cyanoacrylate encapsulated xylitol with a core-shell ratio of 58.6 %.<sup>9</sup> Their

data shows a reduction of the storage capacity of their material from 243 J·g<sup>-1</sup> (before coating) to 115 J·g<sup>-1</sup> (after coating). Similar problems occur in the work of Rezvanpour and coworkers<sup>13</sup> and Zhu and coworkers<sup>14</sup>. Rezvanpour *et al.* used *n*-icosane as core and poly(methyl methacrylate) as shell material. Their results show a reduced thermal storage capacity from 202 J·g<sup>-1</sup> (before coating) to 125 J·g<sup>-1</sup> (after coating).<sup>13</sup> Zhu *et al.* prepared silica-polydopamine-silver nanoparticle coated *n*-octadecane. They report a decrease in the thermal storage capacity from 202 J·g<sup>-1</sup> (before coating) to 72 J·g<sup>-1</sup> (after coating), which was even more reduced when the silver nanoparticle concentration was increased.<sup>14</sup> Therefore, the core to shell ratio can be considered a critical factor in the preparation of encapsulated PCMs.

Remarkably, little attention has been paid to a technique that is known to produce ultrathin coating layers, thus promising high core to shell ratios. Layer-by-layer (LbL) coatings have been used for manifold applications because of their simplicity and ability to produce self-assembled shell structures that can be as thin as several nanometers per layer. Richardson and coworkers provide an overview of the possibilities of LbL coatings.<sup>15</sup> Originally, polymeric LbL coating emerged from the use of electrostatic interactions of polyanions and polycations.<sup>16</sup> More advanced techniques make use of van der Waals interaction in employing stereocomplex formation for the LbL thin film preparation. Serizawa *et al.* used isotactic (*it*-) and syndiotactic (*st*-) poly(methyl methacrylates) (PMMA) for a stepwise buildup of self-assembled thin stereocomplex films.<sup>17</sup> They report a film thickness of 9.7 nm on a quartz crystal microbalance

(QCM) substrate after 20 assembly steps. The same group reported various possible applications for this stereocomplex in biomedical fields.<sup>18</sup> A deposition approach using an inkjet system was also reported.<sup>19</sup> In the previous chapter, the above-mentioned advantages of LbL coatings were directed to thermal energy storage and employed *it*-PMMA and *st*-PMMA for the stereocomplex coating of pentaerythritol, an organic sugar alcohol PCM.<sup>20</sup> The preliminary results at that time gave further issues to improve, such as the solubility combination between the PCM and polymers, as well as the selection of the LbL polymers.

Corresponding to the learnings from the previous chapter, this chapter makes use of polyelectrolytes instead of stereoregular polymers as coating. This is also a result of the different core material applied here. By changing from a hydrophilic core to a hydrophobic one, it is possible to exchange the potentially harmful organic solvents for the coating polymers by water, which is a good solvent for the here used polyelectrolytes. Moreover, the electrostatic interactions used to complex the polyanions and polycations are expected to be formed easier as they do not require similar special rearrangement for the complex formation as isotactic and syndiotactic PMMA would.

The commonly understood principle behind the stepwise layer buildup of polyelectrolytes is based on a charge inversion upon absorption of the successive layer. For example, if a negatively charged polyanion is absorbed onto a positively charged polycation layer, the positive charges are compensated and in the ongoing process, a charge inversion

occurs on the surface. The polymers in solution now have the same charge as the underlying polymer layer and thus the adsorption process is halted by self-regulation. Experimentally, the phase inversion is often observed by measuring the theta potential. In the described process, the complete phase inversion on the coating surface is confirmed by theta potential alternating between positive and negative values.

Interestingly, the thickness of successively adsorbed layers of poly(acrylic acid) (PAA) and poly(allylamine) (PAH) (Figure 3-1) have been found to be tunable by adjusting the pH of the polymer solutions for adsorption, making these coatings highly customizable (Figure 3-2).<sup>21</sup>

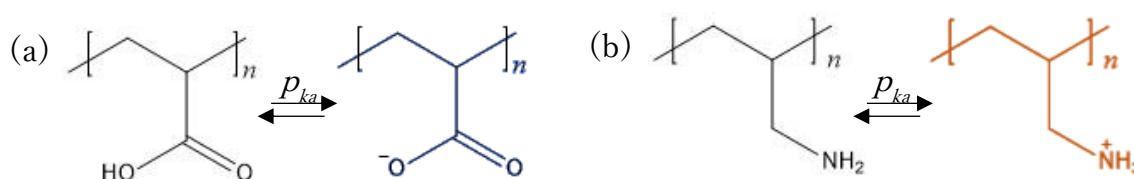


**Figure 3-1:** Chemical structures of icosane (a) and poly(acrylic acid) (b) (counter ions omitted).

From Figure 3-2 it can be seen that the region between pH 4.5 and 6 is yielding the highest layer thicknesses. The reason for this behavior can be found in the charge density of PAA and PAH polymer chains in this pH range.<sup>21</sup> PAH on the one hand is fully charged in the pH region between 5.5 and 6. PAA on the other hand is close to fully charged state at about 80 to 90 %, but still shows some protonated carboxyl groups. According to Shiratori and coworkers, this condition yields the highest increase in layer thickness during the deposition steps because of

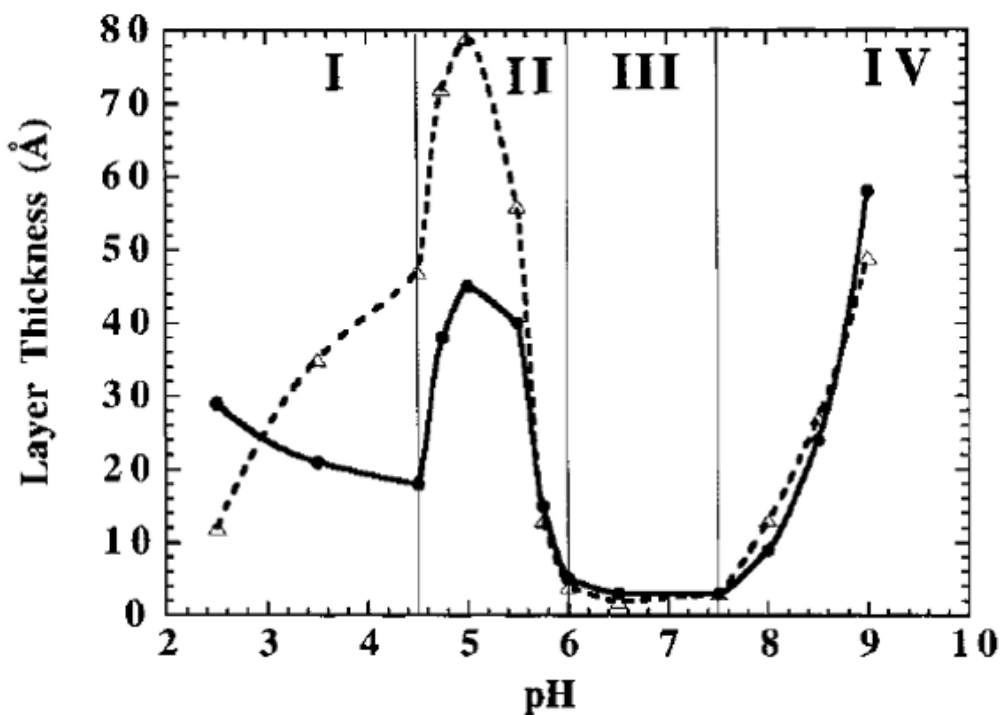
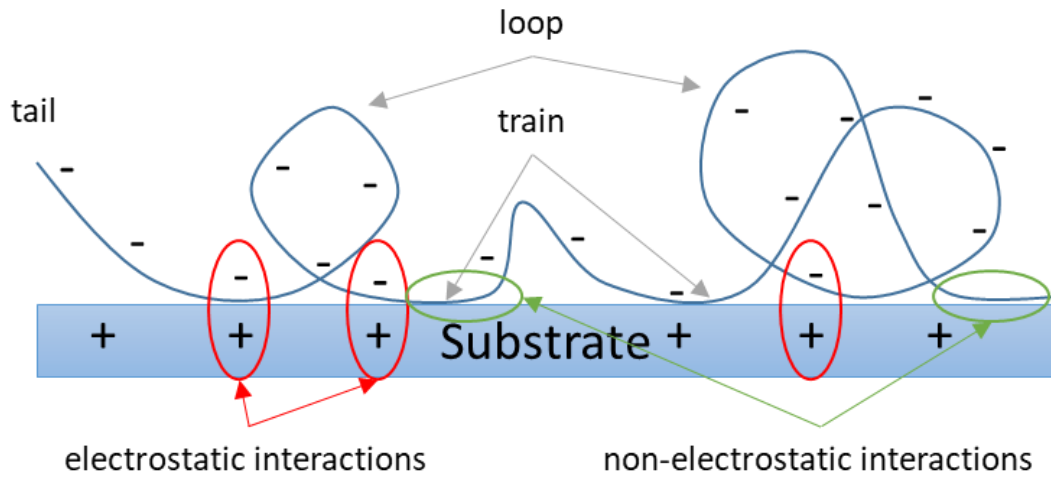


**Figure 3-2:** Schematic illustration of the configuration of adsorbed polymers on a substrate (upper part); pH dependent layer thickness increase of polyelectrolyte multilayers assembled from PAA and PAH solutions at the same pH (lower part). Reprinted with permission from Shiratori et al. *Macromolecules*. 2000, 33, 4213-4219. Copyright 2000 American Chemical Society.<sup>21</sup>

the arrangement of the adsorbed polymers and the specific distribution of trains, loops and tails of the adsorbed polymer chains with a typical segmental increase in the loop population (Figure 3-2, upper part). Furthermore, layered PAA/PAH can be cross-linked by turning the electrostatic

interactions into amide bonds, providing increased stability over a wide pH range and significantly decreased permeability compared to films lacking these covalent bonds (Figure 3-4).<sup>22</sup>

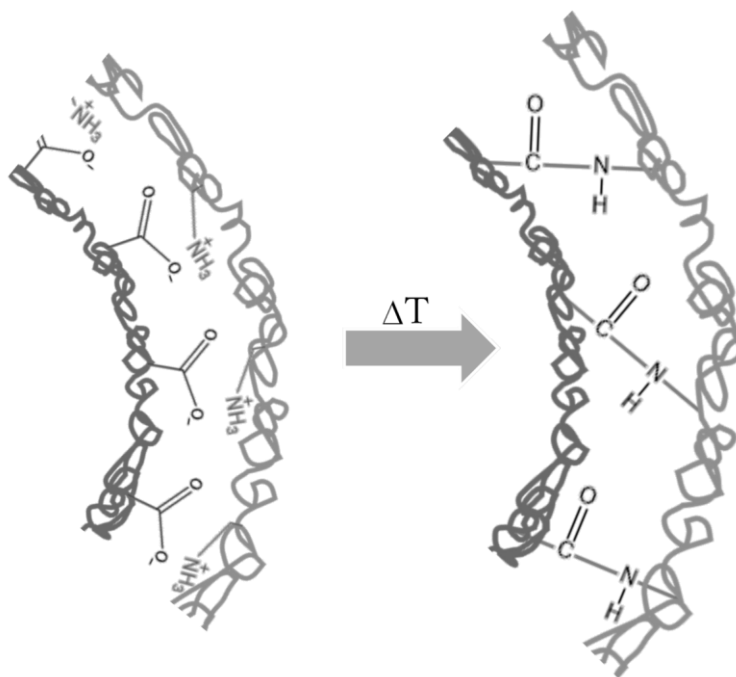


**Figure 3-4:** Thermal crosslinking via amide-bond formation is an attractive option to increase the stability.

Concerning the core material, paraffin-type substrates like octadecane<sup>23</sup>, hexadecane<sup>24</sup> or icosane<sup>25</sup> have already successfully been encapsulated in several PCM coating approaches. By switching the core material from pentaerythritol in previous studies to icosane, the application temperature of the PCM capsules was shifted close to body temperature. Moreover, icosane's hydrophobic properties facilitate the coating process, as it is not soluble in the polyelectrolyte-water coating solutions. In general, reports of using LbL self-assemblies to coat PCMs for thermal energy storage seem to be rather rare. Only three other publications in this field could be found. Of these three, only one describes a general approach, while the other two

are very specific, targeting the functionalization of a cotton fabric for smart textiles<sup>26</sup> or pursuing intentions to combine carbon capture and utilization and energy storage<sup>27</sup>. Only Yi and coworkers presented a more general approach for the encapsulation of octadecane droplets by three double layers of poly(styrene sulfonate) (PSS) and poly(diallyldimethylammonium chloride) (PDADMAC) using bovine serum albumin as a surfactant.<sup>28</sup> According to their calculations, their resulting encapsulated PCM contains 91.3 mass-% of octadecane and a storage capacity of 172.84 J·g<sup>-1</sup> after coating compared to 189.21 J·g<sup>-1</sup> before coating.

In this chapter, the use of PAA and PAH as electrostatically interacting shell materials for the LbL coating of icosane as a novel PCM is reported. In contrast to the examples mentioned above<sup>26-28</sup>, the cross-linking of PAA and PAH via amide bond formation for the stabilization of PAA/PAH covered capsules was assessed. Considering the nature of the surfactant, didodecyldimethylammonium bromide (DODAB), bearing two long alkyl chains

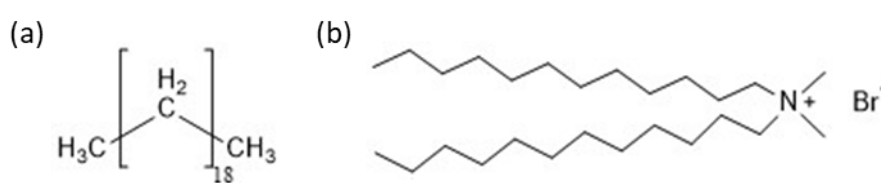


**Figure 3-5:** Chemical structures of icosane (a) and DODAB (b).

and a single positive charge per molecule (Figure 3-5), is a suitable choice and a good basis for the successive layer buildup. For these reasons, the present approach is flexible and can be expanded for use with various paraffin-type PCMs. In this chapter, icosane is used as a PCM. Due to its melting region, possible applications in solar air collectors equipped with thermal

storage units with respect to regional climate conditions are expected.<sup>29</sup> This is the first report of the layer-by-layer coating of icosane by weak polyelectrolytes poly(acrylic acid) and poly(allyl amine) to be used as a phase change material for thermal energy storage.

## **3.2 Experimental**

### ***3.2.1 Materials***

Poly(acrylic acid) (PAA,  $M_w$  250 000, Wako, Japan), Poly(allylamine) hydrochloride (PAH,  $M_w$  50 000, Aldrich, Japan), Didodecyldimethylammonium bromide (DODAB, 98 %, Aldrich, Japan), Icosane (>98 %, TCI, Japan), Rhodamine B (RhB, >95%, Aldrich, Japan) and NaOH (1M, Nacalai Tesque, Japan) were purchased and used without further purification. H<sub>2</sub>SO<sub>4</sub> (98 %, Wako, Japan) and hydrogen peroxide (30 %, Wako, Japan) were used for the preparation of piranha solution used in the QCM experiments. D<sub>2</sub>O was purchased from SCETI K.K, Japan.

### ***3.2.2 Determination of the experimental conditions***

Several preliminary adjustments and trials were performed before the final experimental setup was decided. First, water was determined as the best solvent for the polyelectrolytes as it is dissolving the hydrophilic polyanions and polycations easily. Moreover, it is environmentally friendly and does not have harmful effects on the human body especially



in comparison to organic solvents. Second, compared to the particle preparation approach in the previous chapter, a different approach was chosen. Here, an emulsion technique was used to prepare the particles. This is an improvement compared to the previous chapter, because it is assumed that the spherical particles are easier to adsorb the polymers homogeneously because of their uniform surface. Moreover, by using a suitable surfactant that can provide the particle surface with a charge, an anchoring point for the first polymer layer can be created and the adsorption process can be facilitated.

The surfactant was chosen among sodium dodecyl sulfonate (SDS), didodecyldimethyl ammonium bromide (DODAB), bovine serum albumin (BSA), dodecanol (lauryl alcohol) and lauric acid. Emulsions of icosane and surfactant were prepared at various concentrations and their stability was evaluated by eye before and after centrifugation. The LbL approach used herein is on the one hand highly dependent on the dispersion of the particles in the solutions, so they do not aggregate. On the other hand, the particles must be collected in the centrifugation step and thus, the emulsion must satisfy both of these criteria. Therefore, the primary objective during the particle preparation was not to exactly determine the particle size via the adjustment of the emulsion parameters, but to prepare an emulsion, which would satisfy the above-mentioned requirements. In this case, DODAB was chosen as the suitable surfactant.

After the surfactant was decided, the molecular weight and concentration of the coating polyelectrolytes was adjusted. The pH was controlled according to the above given explanations.

The concentration was first evaluated among polymer solutions of 2, 5 and 10 mg/ml in water. To reduce polymer consumption and because the higher molecular weight PAA was difficult to dissolve at high concentrations, conditions were adjusted at 2 mg/ml. While the weight for PAH was kept constant, the  $M_n$  of PAA was varied between 25 000, 250 000 and 1 000 000. A combination of PAH ( $M_n = 50\ 000$ ) and PAA ( $M_n = 250\ 000$ ) was finally selected for the particle preparation due to the stability during DSC measurements. It is not fully clear, why the other combinations failed at the DSC experiments and could not contain the icosane loading. A possible explanation could be found in the chain length. At a  $M_n$  of 25 000, the PAA chains seem to be too short to form a stable coating with the PAH layers, whereas at a molecular weight of 1 000 000, the chains might not assemble well on the underlying layer and create too many loops and tails so that the final layered structure becomes unstable. However, the confirmation of these assumptions will not be part of this thesis, as it was only desirable to find a stable condition, which was finally achieved.

### ***3.2.3 Particle preparation***

DODAB was used as a surfactant to create oil-in-water emulsions according to a procedure proposed elsewhere.<sup>30</sup> Therefore, 1 ml of icosane was prepared in a 100 ml glass vial and 50 mg/ml surfactant was added. The mixture was heated by combined plate heater/stirrer (HHE-19G-US, KPI, Japan) to 50 °C until all the icosane melted. Then, 30 % (v/v icosane)

chloroform was added to dissolve the surfactant in the icosane melt. After this process had been completed, 63.7 ml of preheated (50 °C) ultrapure water (18.2 Ω, from Direct-Q 3UV, MerckMillipore, Japan) was added to sum up for a total volume of 65 ml. This pre-emulsion was stirred by magnetic stirrer for 10 min and then sonicated at 50 °C for 30 min at (40 kHz, MCS-3, AS One, Japan) to create the final milky-white emulsion. The emulsion particles were received by freeze-drying the emulsion after sonication, using liquid nitrogen and a freeze-drying apparatus (FDU-1200, Eyela, Japan) to remove the water completely.

### 3.2.4 Particle coating

Particle coating was done by consecutively submersing the particles into polymer solutions of PAA and PAH, including a washing step by ultrapure water in between – a standard procedure for LbL coating. The process is schematically illustrated in Figure 3-6.

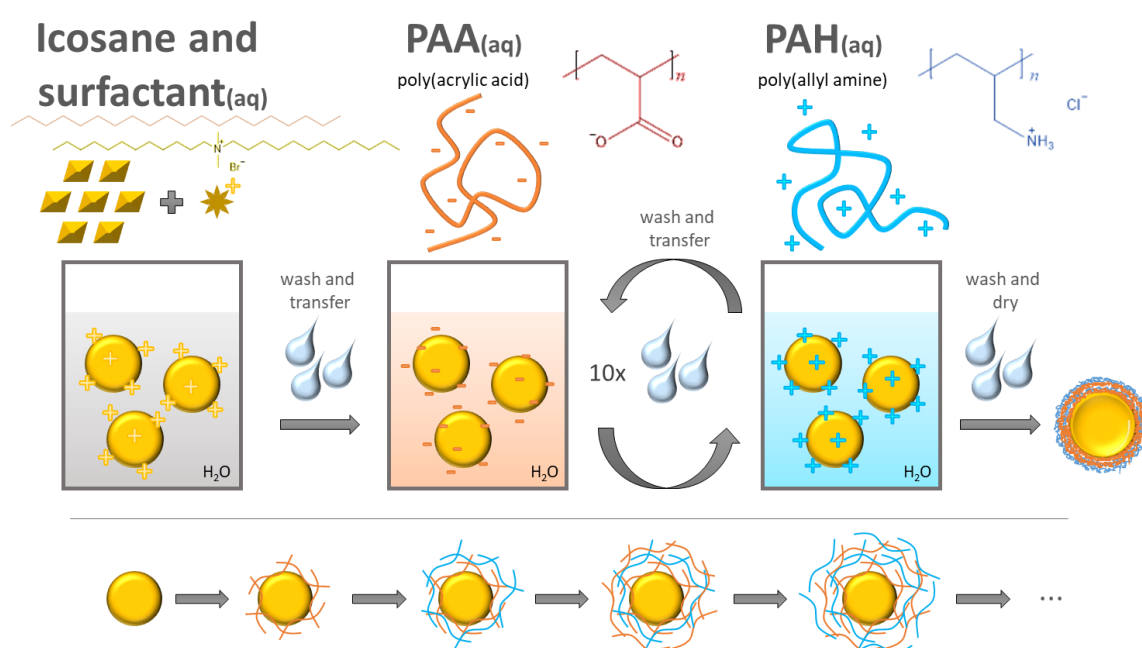


**Figure 3-6:** Schematic illustration of the coating process and the stepwise layer growth.

Briefly, polyelectrolyte solutions were prepared separately using 2 mg/ml in ultrapure water and pH was adjusted to 5.7 in both solutions by 1M NaOH. In each coating step, 10 ml of fresh polymer solution was used. The emulsion particles prepared in the first step, bearing the positive charge of the surfactant, were first immersed into the polyanion solution. The resulting suspension was clipped onto a bio shaker (V-BR-36, Taitec, Japan) and moved for 5 min at room temperature to prevent aggregation. It is considered that this is an appropriate coating time for the electrostatic interactions to establish (see QCM data in the following section). After that, the suspension was centrifuged to recover the particles at 3500 rpm for 5 min at room temperature (Kubota6200, Kubota, Japan). As the particles' density is lower than that of the polymer solution, the particles, which were floating on the top of the vial, could be easily separated by removing the underlying solution by pipette, which was carefully inserted through the particle layer. Following this, the remaining particles were re-dispersed in 10 ml of ultrapure water to remove remaining or only weakly attached polymers. The water was removed again by the centrifugation process described above, and this washing process was repeated for three times in total. This process is considered one coating step. Repeating the same process for the polycation solution completed the first coating cycle, resulting in the first polyanion-polycation double layer. When finally a number of 10 cycles were completed (equal ten double layers), the particles were recovered, freeze-dried and kept for further analysis.

### **3.2.5 Characterization**

The general buildup of the polyanion-polycation layers was checked by Quartz Crystal Microbalance (QCM, parent frequency 9 MHz, USI, Japan). Particles were analyzed by Fourier-transform infrared (FT-IR, IR Affinity-1S, Shimadzu, Japan) for confirmation of the coating. All measurements were recorded in wavenumber from 400 to 4000  $\text{cm}^{-1}$  with a resolution of 4  $\text{cm}^{-1}$  and accumulated over 512 times. Further analysis of the shell structure was performed by nuclear magnetic resonance ( $^1\text{H}$  NMR, ECX-400P, JEOL, Japan) measurement in  $\text{D}_2\text{O}$ . The coated particles were washed with hexane before the measurement to remove the icosane core and improve the signal strength. Furthermore, NaCl was added to break up electrostatic interactions in the shell complex and increase the solubility. Measurements were conducted at 400 MHz, room temperature and recorded with an accumulation of 128 scans for PAA and PAH and 4096 scans for the coated samples. A fluorescence microscope (TCM 400FLR, Labomed, USA) was used to evaluate the shell structure under Rhodamine B (RhB) staining using a dichroic mirror with a transmission of 93 % at wavelength of 540 nm and onwards. Therefore, a 2mM aqueous solution was prepared and coated particles and pristine icosane were stained for 5 min in the solution under shaking. Then, RhB was washed three times with water over a filter to obtain the stained samples, which were dried on the specimen holder. Pictures were taken by CCD camera (Buffered USB CCD Camera, Mightex, Canada). Structural characterization was further carried out using scanning electron microscopy (SEM,

SU6600, Hitachi, Japan). SEM images were taken at an acceleration voltage of 2 kV at approximately 10 mm working distance. Thermal properties were evaluated by thermogravimetric analysis (TGA, TGA-50, Shimadzu, Japan) and differential scanning calorimetry (DSC, DSC-60Plus, Shimadzu, Japan) including cycling experiments to judge the particles long-term stability. TGA was conducted at a heating rate of  $10\text{ }^{\circ}\text{C}\cdot\text{min}^{-1}$  up to  $500\text{ }^{\circ}\text{C}$ . DSC measurements were made at  $2\text{ }^{\circ}\text{C}\cdot\text{min}^{-1}$  or  $10\text{ }^{\circ}\text{C}\cdot\text{min}^{-1}$  between  $10\text{ }^{\circ}\text{C}$  and  $60\text{ }^{\circ}\text{C}$ . Data used in this work relates to the second heating and cooling cycle. TGA and DSC measurements were carried out under nitrogen flow at  $100\text{ ml}\cdot\text{min}^{-1}$ . Moreover, heating experiments under nitrogen atmosphere were conducted to evaluate the coating stability, and solubility experiments gave insight into the coating's protection abilities against solvents for the core.

### **3.3 Results and Discussion**

In contrast to so called strong polyelectrolytes like PSS and PDADMAC that are always fully dissociated in solution, the layer properties of films build up from weak polyanions and polycations strongly depend on the protonation and deprotonation of the materials and thus on the pH of the polyelectrolyte solutions. Therefore, it is possible to tune the layer thickness to a certain degree by adjusting the pH accordingly.<sup>21,31</sup> Another important factor for the stepwise deposition during the LbL process for both, weak and strong polyelectrolytes, is the

dipping time, during which the self-assembly of subsequent layers is happening on top of the substrate.

### **3.3.1 Structural evaluation**

#### **3.3.1.1 Quartz Crystal Microbalance (QCM)**

QCMs are based on a quartz crystal resonator. If a polymer (or any other kind of material) is adsorbed onto the surface, the resonance frequency of the crystal will change. Using Sauerbrey's equation, the obtained frequency shift can be translated to the corresponding mass at the nanogram order depending on the resolution of the applied system.<sup>32</sup> To confirm the adsorbed amount of polyelectrolytes in each coating step and to judge the adjusted coating conditions, the layering process was monitored by QCM. LbL coating of QCM by PAA/PAH has been reported elsewhere<sup>31</sup>, but setting similar concentrations (2 mg/ml) of polymer solutions and identical pH values (pH 5.7) compared to the actual particle coating allowed to evaluate the suitability of our chosen conditions. During the coating process, a stepwise adsorption of polyanions (PAA,  $M_w$  25 000) and polycations (PAH,  $M_w$  50 000) respectively could be observed on the QCM substrate, monitored by the shift in the oscillation frequency of the quartz crystal (Figure 3-7). Sauerbrey's equation (Equation 3-1), was used to calculate the adsorbed masses in the nanogram order accordingly.

$$\Delta f = \frac{2f_0^2}{A\sqrt{\rho_q\mu_q}} \Delta m \quad \text{Equation 3-1}$$

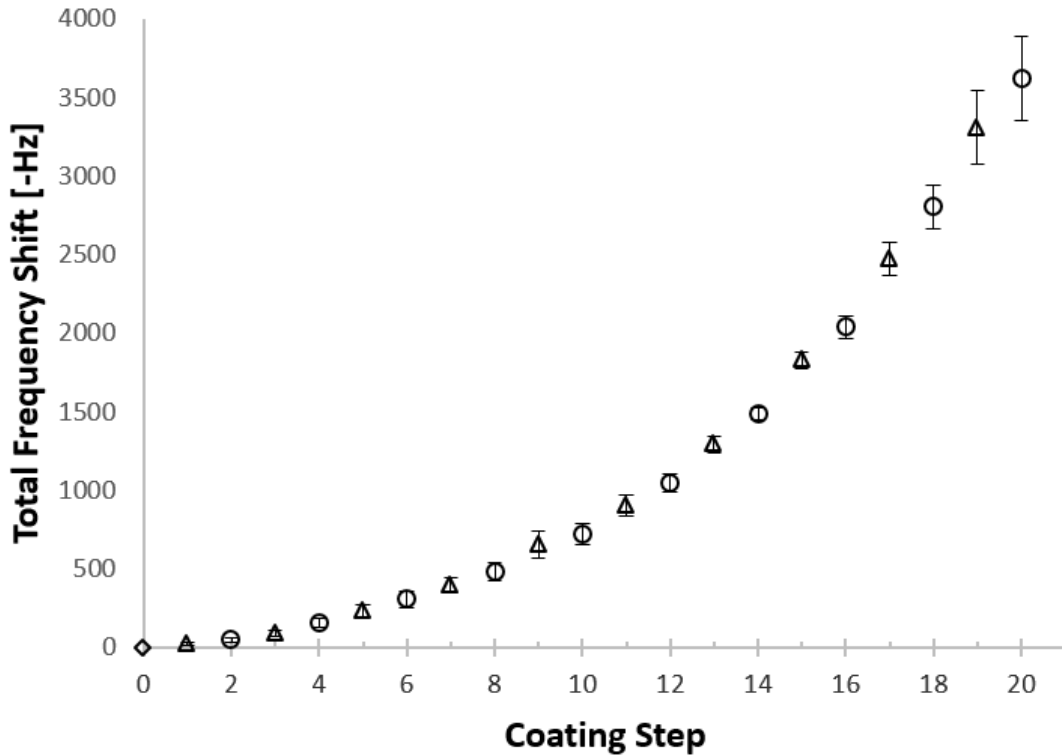


**Figure 3-7:** Oscillation frequency shift of the QCM substrate during stepwise adsorption of oppositely charged polyelectrolytes. Diamond symbolizes the measurement of the blank QCM ( $\diamond$ ) and triangle and square symbolize the absorption steps of PAH ( $\Delta$ ) and PAA ( $\circ$ ) respectively. Error bars represent the standard error over the averaged frequency shifts ( $n=3$ ).

As can be seen in Figure 3-1 from step one to nine, the frequency shifts increase slightly with each step, but are considered rather small (increasing between 13 and 270 Hz) compared to the shifts after the tenth step (increasing between 108 and 721 Hz). The corresponding amounts of polymer adsorbed in the lower steps range from 11 to 234 ng. In the higher steps, adsorbed masses range from 94 to 625 ng per step. There are two growth mechanisms known for the multilayer growth during LbL assemblies – a linear one and an exponential one. The linear growth is achieved when the polymers for each layer are rather stiff and straightened out. Polymers that are more flexible on the other hand are able to penetrate into the underlying network via diffusion, causing rearrangement of the already adsorbed layers, which results in



exponential growth.<sup>33</sup> This behavior can be seen in Figure 3-7. The first steps are rather small compared to the later steps as explained before. That is because in the beginning, there is no possibility for the polymers from the next step to diffuse into a underlying network as it is not yet built. In the later steps however, the polymers from the next coating step can diffuse into the already grown multilayers, which is the reason for the observed exponential growth. As reported by Bieker *et al.*<sup>31</sup>, the LbL approach is good to control the amount of adsorbed polymer on the films in each step according to the chosen pH of the polymer solutions. In their experiments, the thickest layers were obtained in the region from pH 4.5 to 6. By setting the pH to 5.7, higher adsorbed amounts can be expected compared to other pH regions (Compare Figure 3-2). This is reflected in the high frequency shifts measured. Nevertheless, the overall adsorbed masses will be small compared to the encapsulated icosane. From these results, it was expected that the LbL condition of 20 steps (10 cycles) at the given pH is suitable to achieve coatings thin enough to prepare highly efficient encapsulation of PCM.

### 3.3.1.2 Scanning Electron Microscope

After getting insight into the assembly behavior of PAA/PAH by QCM, the particle coating process was applied as described above and finally the coated particles were obtained after 10 cycles, which were determined by QCM results. A first estimation about the success of the coating process was done by evaluating SEM images. Figure 3-8 shows a comparison of

the particles before coating, containing only icosane and DODAB surfactant (Figure 3-8a and 3-8b) and the coated particles consisting of icosane-DODAB-(PAA/PAH)<sub>10</sub> (Figure 3-8c and 3-8d) both after freeze drying at varying magnifications.

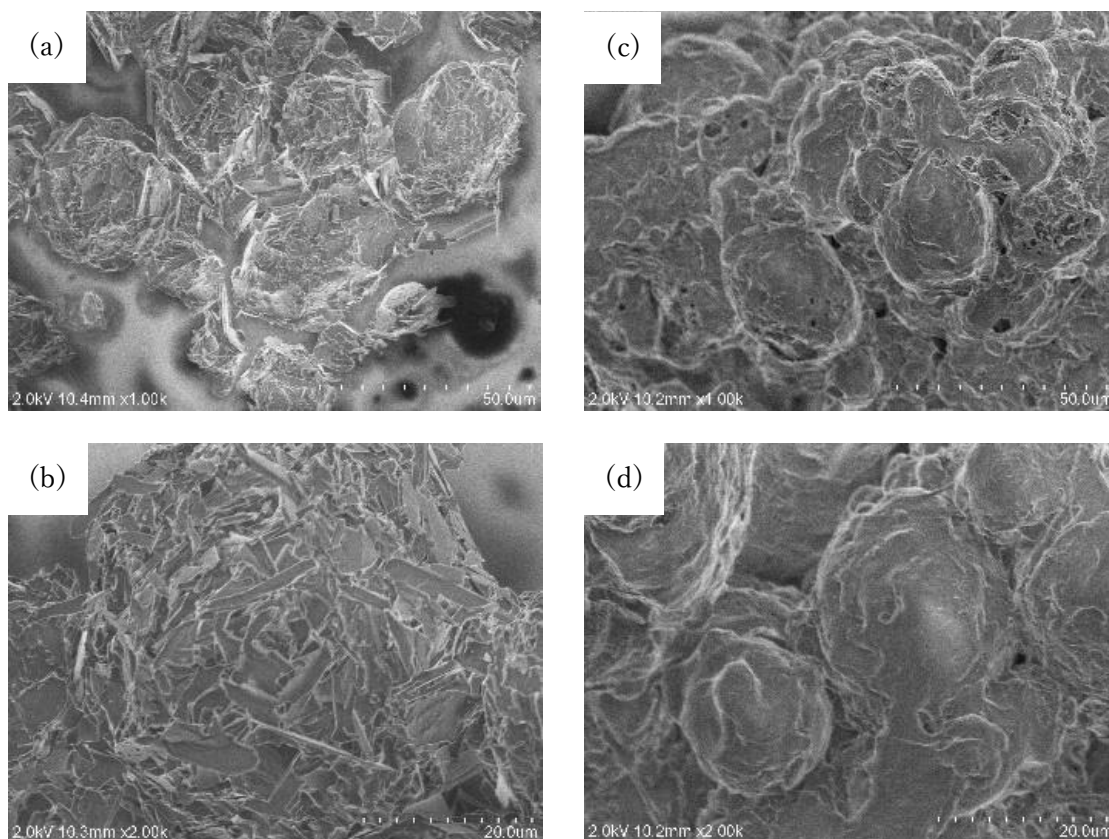


**Figure 3-8:** SEM images of coated and uncoated particles at different magnifications. (a) Icosane-DODAB, x1000, (b) icosane-DODAB, x2000, (c) icosane-DODAB-(PAA/PAH)<sub>10</sub>, x1000 and (d) icosane-DODAB-(PAA/PAH)<sub>10</sub>, x2000.

Very obviously, the uncoated particles are spread out more homogeneously (Figure 3-8a), while the coated particles display some aggregation (Figure 3-8b). This is due to some small amount of coating polymers that might have spread over adjacent particles, thus weakly connecting them. Usually, complete charge reversion at the particle surface is expected upon addition of successive layers, stabilizing the particles in suspension and preventing aggregation through electrostatic repulsion. A possible explanation could be the stronger gravitational forces during

centrifugation, allowing the particles to approximate close enough for the coating polymers to bridge over and connect adjacent particles. This would also reduce the free charge density on the surface, reducing the electrostatic repulsion and allowing the particles to stay connected through the bridging. Additionally, the particle size might be large enough to ignore the electrostatic repulsion, at least partially. As the particles are nevertheless clearly observable individually, it is concluded that this connection might only have formed at a very late stage of the coating, probably in the last steps. Therefore, it is further assumed that the underlying particles are homogeneously coated and that this weak aggregation does not affect the encapsulation efficiency directly. Further hints of the encapsulation and formation of a shell are very small “holes” (dark spots) in the coated particles’ surface indicating occasionally incomplete shell formation (Figure 3-8c). These holes are not present on the surface of the uncoated particles. Judging from at least five different images, the average particle size of the spherical particles is homogeneously distributed around 20 to 50  $\mu\text{m}$ , which is a suitable value for encapsulated PCMs, concerning the heat transport from the outside to the center of the core. Another observation that can be made is the difference in the surface structure of coated and uncoated particles. While the uncoated particles show a rough and rugged surface (Figure 3-8b), the coated particles are rather smooth (Figure 3-8d). In Figure 3-2b small platelet-shaped structures are visible on the particles, which can be attributed to the crystal structure of the icosane core material. The long alkyl chain arms of the DODAB surfactant should not

negatively interfere with the crystallization process of icosane. A completely different situation is presented in Figure 3-8d. The surface of the coated particles does not show the rough and rugged structures of the uncoated particles, but displays rather smooth areas with no signs of the underlying core material. The difference becomes even clearer at x2000 magnifications. It is hypothesized that smoother coatings could be obtained by increasing the number of layers, but that this would result in significant bridging and ultimately lead to the formation of large aggregates. Therefore, it is concluded that using ten coating cycles provides high enough amounts of shell material for robust encapsulation and at the same time, low enough amounts to enable high efficiency of the PCM.

### *3.3.1.3 Fourier-Transform Infrared Spectroscopy*

After checking the topological appearance by SEM, FT-IR spectra of the coated material and of the starting materials were evaluated to refine the structural characterization.

The resulting spectra are shown in Figure 3-9.

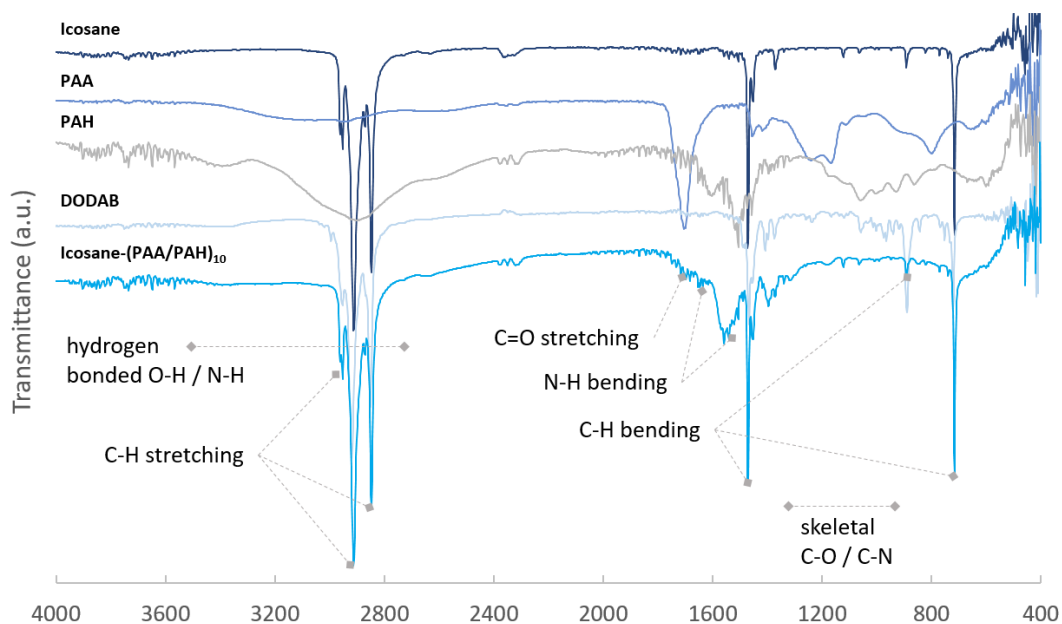


**Figure 3-9:** FT-IR spectra of starting materials and final icosane PCM encapsulated by ten double layers of PAA-PAH. Spectra are labelled as (a) icosane, (b) PAA, (c) PAH, (d) DODAB and (e) icosane-DODAB-(PAA/PAH)<sub>10</sub>.

The starting materials can be distinguished by their characteristic peaks and as expected, these peaks reappear in the coated particles, hinting at a successful coating. The strong peaks of the icosane core material appear at identical wavelengths in the coated particles, and are clearly visible at  $2953\text{ cm}^{-1}$ ,  $2913\text{ cm}^{-1}$  and  $2847\text{ cm}^{-1}$  and are assigned to C-H stretching (Figure 3-9a and 3-9e). Additionally, the peaks at  $1472\text{ cm}^{-1}$  and  $716\text{ cm}^{-1}$  are assigned to C-H bending. The carbonyl C=O peak of polyanion coating material PAA can be found at  $1703\text{ cm}^{-1}$  (Figure 3-9b) and at  $1705\text{ cm}^{-1}$  in the coated particles' spectrum respectively, although it almost completely vanished possibly due to the strong interaction with the polycationic PAH (Figure 3-9e). PAH displays strong N-H bending peaks around  $1506\text{ cm}^{-1}$  and  $1558\text{ cm}^{-1}$  (Figure 3-9c) which appear at the same wavelengths in the coated particles (Figure 3-9e). Two C-H peaks marking the presence of DODAB surfactant (Figure 3-9d) in the coated particles are presented at  $891\text{ cm}^{-1}$  and  $1397\text{ cm}^{-1}$ , appearing in pristine DODAB at  $889\text{ cm}^{-1}$  and  $1397\text{ cm}^{-1}$

respectively (Figure 3-9e). During the coating process, several washing steps were performed. Therefore, loosely connected or free starting materials should not exist in our coated particles.

Thus, the discovery of the specific peaks of the starting materials in the coated particles is a strong indication for the successful coating. Moreover, the large group of peaks in the range of  $1500\text{ cm}^{-1}$  to  $1600\text{ cm}^{-1}$  of the coated material can be assigned to the strong interaction of the carboxyl and amine groups of the polyelectrolyte coating materials (Figure 3-9e). Thus, the appearance of this group is caused by partially shifted peaks from the carbonyl region of PAA at  $1703\text{ cm}^{-1}$  and from the amine peaks, which we assigned at  $1558\text{ cm}^{-1}$ , to this position.

#### *3.3.1.4 Characterization of the shell structure*

To further confirm the chemical structure of the shell,  $^1\text{H}$  NMR measurements were performed. Spectra of PAA, PAH and hexane washed, encapsulated particles were obtained and compared (Figure 3-10). The hexane washing was used to remove the icosane core from the capsules and to improve the samples signal strength.

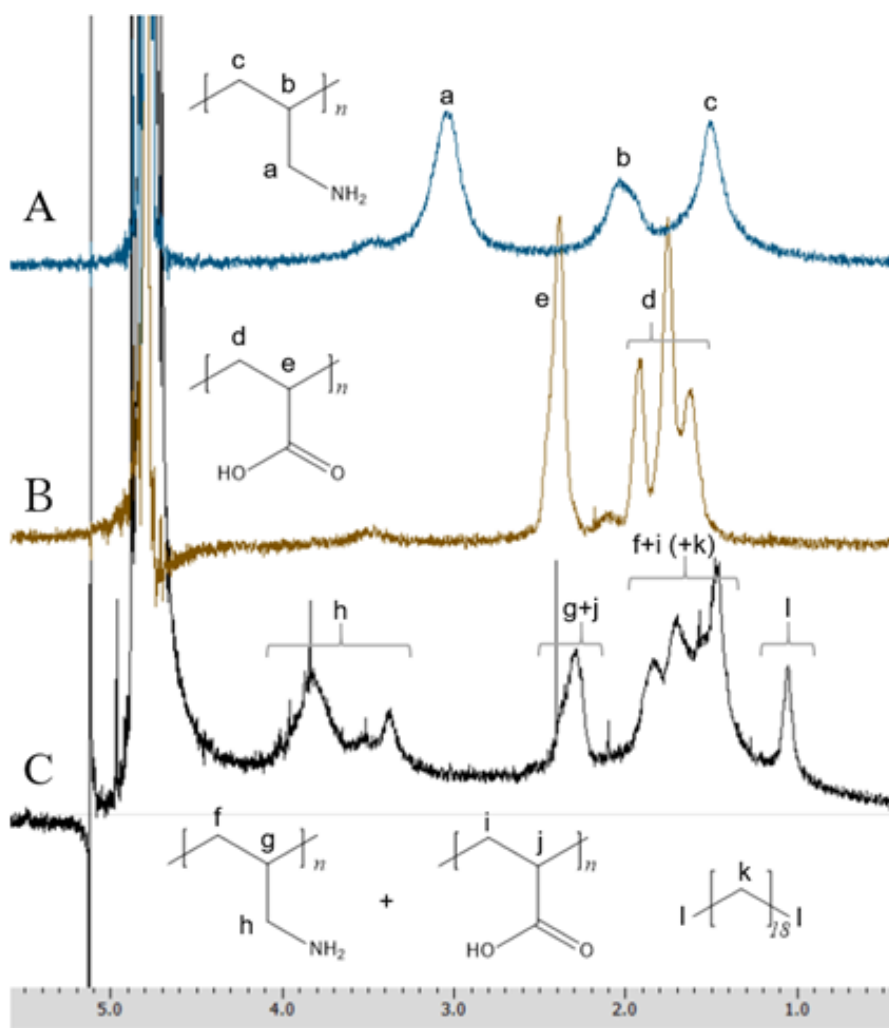


**Figure 3-10:** <sup>1</sup>H NMR-spectra of PAH (A), PAA (B) and the coated particles in D<sub>2</sub>O (C) (400MHz, room temperature).

The characteristic peaks of the two shell materials, PAA and PAH, were obtained, slightly shifting from their original value, which is a hint for their strong interaction to form a film. Figure 3-10A shows the <sup>1</sup>H NMR spectrum of PAH, where peak a at 3.047 ppm marks the two protons of the allyl arm, while peak b at 2.037 ppm and peak c at 1.505 ppm mark the protons of the polymer backbone. Accordingly, peaks e at 2.382 ppm and d at 1.918, 1.751 and 1.641 ppm in Figure 3-10B have been assigned to the polymer backbone of PAA. The <sup>1</sup>H NMR spectrum of the coated and hexane-washed particles finally is presented in Figure 3-10C. We

assume the shifting and combining of peaks because of the interaction of the two polymers during the shell formation as follows. Peak a is reflected in position h, while peaks b and e can be found combined in position g+j. Peaks c and d are assigned for position f+i. The peak at position l might stem from residual icosane, which was not completely removed. This residue would also cause some additional signal in position f+i (+k). In all spectra of Figure 4, the large peak at 4.790 ppm is assigned as the solvent peak for D<sub>2</sub>O. In General, the peak signal of the coated particles must be considered very weak and needed overnight measurement to be accomplished. Therefore, the results of this evaluation must be considered carefully. The peaks of PAA (Figure 3-10B) are slightly shifted upfield, indicating a stronger shielding effect. Contrary, the combined peaks appear further downfield compared with the original peaks of PAH (Figure 3-10A), indicating that the protons were deshielded. Although a peak shift is observable and the resemblance of the free polymer peaks with the complexed polyelectrolyte on icosane peaks is obvious, it is difficult to explain the observed behavior in detail. In case of the confirmation of the successful encapsulation, FT-IR spectra provide a much clearer image. Nevertheless, additional confirmation of the encapsulation was achieved as follows:

Fluorescence microscopy was used to monitor the shell in comparison to pristine icosane. Therefore, Rhodamine B (RhB) was used as a dye for staining the samples. In Figure 3-11, no fluorescence was detected for the pristine icosane samples (upper row) because the charged dye molecules, which are also containing an carboxylic acid functional group did not



interact with the substrate. Contrary to that, coated particles were able to adsorb the RhB staining and their fluorescence can be clearly seen (lower row).

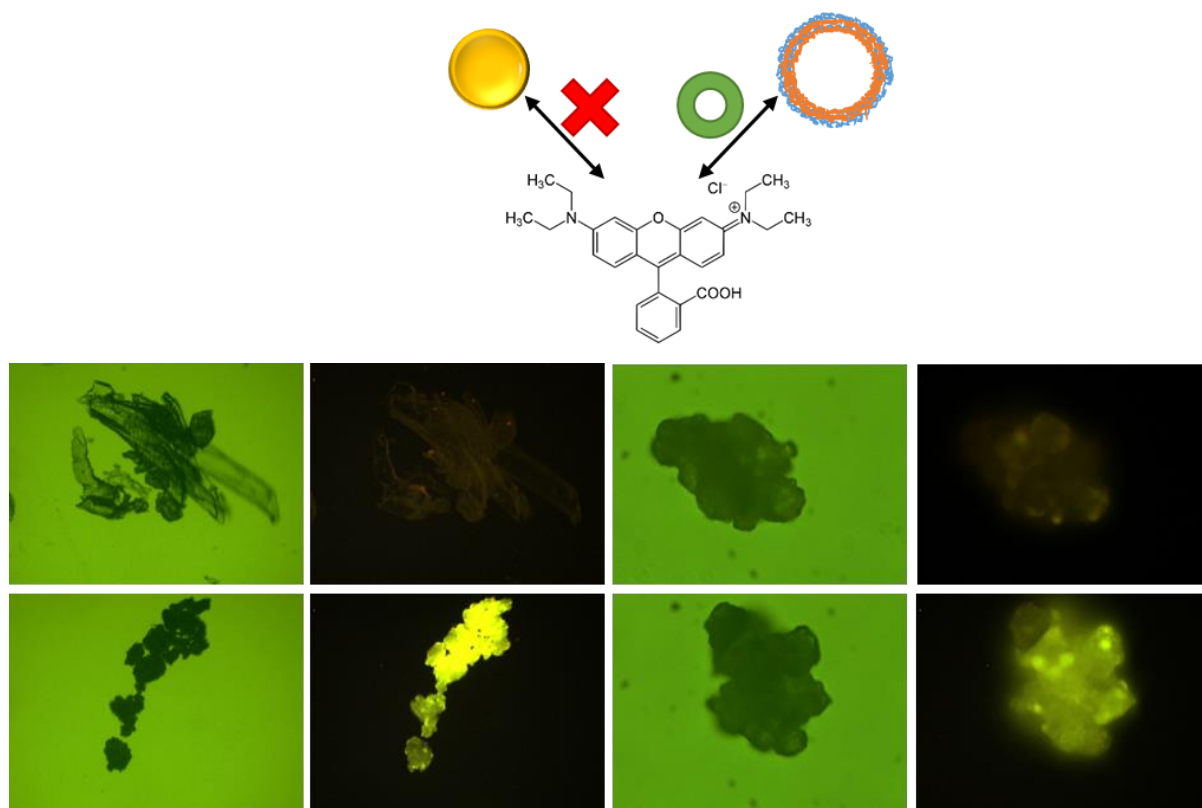


**Figure 3-11:** Schematic illustration of the dye adsorption experiment. Transmission (1<sup>st</sup> and 3<sup>rd</sup> column) and fluorescence (2<sup>nd</sup> and 4<sup>th</sup> column) microscope images of pristine icosane (upper row) and encapsulated particles (lower row) under transmission and fluorescence conditions using a dichroic mirror with a transmission of 93 % at wavelength of 540 nm and onwards.

This is a result of the different chemical nature of core and shell materials and thus is evidence for the diverting shell composition and presence in the encapsulated particles.

### 3.3.2 Thermal properties

After confirmation of the encapsulation by SEM and FT-IR, the influence of the coating on the thermal properties and the thermal storage capacity of the icosane PCM was analyzed.

### 3.3.2.1 Thermal Gravimetric Analysis

TGA was used to gather insight in the thermal degradation behavior of the coated particles compared to their uncoated counterparts. A one-step degradation behavior was assumed for the pure icosane. In comparison to that, the degradation curve of the coated material should at least show a two-step behavior – one-step for the core and another step for the shell. Furthermore and according to previous studies, a slightly higher onset of the thermal degradation was expected. TGA traces are shown in Figure 3-12.

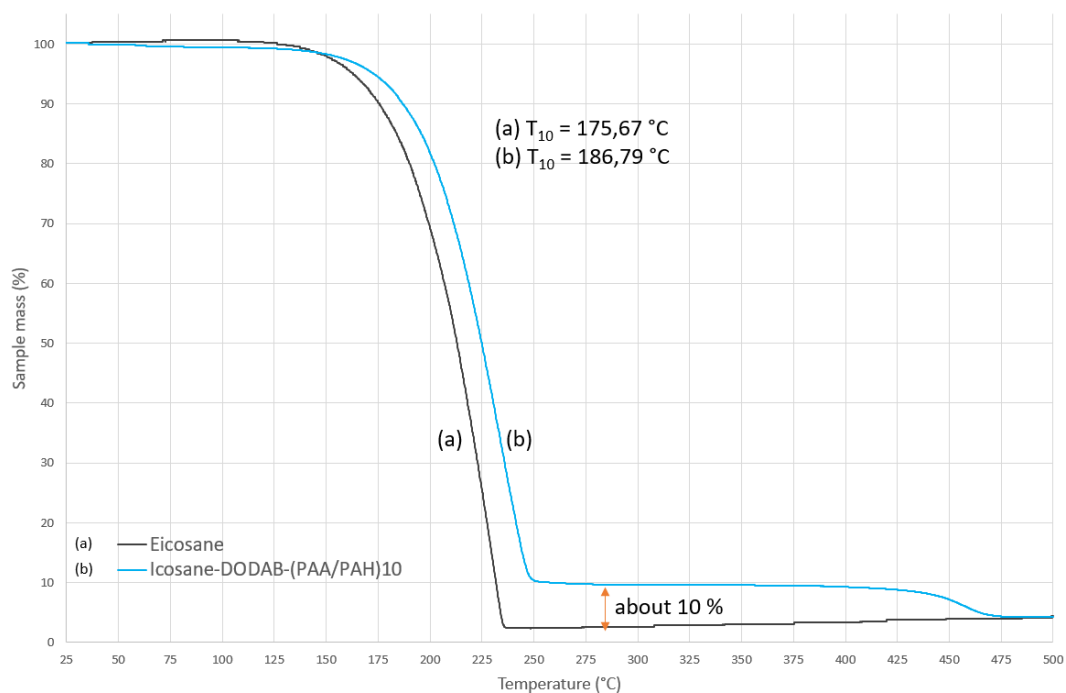


**Figure 3-12:** TGA traces of uncoated (a) and coated icosane (b).

When comparing the traces before and after coating,  $T_{10}$  increased for the coated particle from 175.7 °C (Figure 3-12a) to 186.8 °C (Figure 3-12b). This slightly higher degradation temperature of around 11 °C is due to the protection of the core material by the coating. In general, polymer materials show poor thermal conductivity. In the case of the coated particle,

the heat energy that is arising from the steady temperature increase first needs to be transported through the polymeric coating during the TGA measurement. In that case, it is also reasonable to assume that some bonds in the coating might be broken, which is also reducing the amount of heat energy transferred to the core directly. Thus, the heat transport is slowed down and the degradation is delayed. In case of the uncoated particles, there is no protective polymeric shell and the heat energy can directly attack the icosane core material leading to a faster degradation. Furthermore, a clear two-step degradation mechanism can be observed for the coated particles. This indicates that first the core is affected by the heating, considering that the similarity of the early section of the coated and uncoated particle curves is obvious. This first decrease is followed by a constant region where no weight loss is recorded, indicating the thermal stability of the polymer coating. At a much higher temperature at around 350 °C, the coating material is also affected by the degradation through the heating and the curve starts to decrease again (Figure 3-12b). Interestingly, the difference between the beginning of the second step of the coated particles and the final sample mass of the uncoated icosane is about 10 %, which implies that the amount of core material in the icosane-DODAB-(PAA/PAH)<sub>10</sub> particles is about 90 %. A simplified calculation can show that the height of the coated material can be estimated to be around 500 nm. Overall, weight loss is only observed at much higher temperatures than the intended application range around the melting range of icosane, so no problems for the material caused by thermal degradation are expected.

### 3.3.2.2 Differential Scanning Calorimetry

To expand the thermal characterization, we used DSC to determine the thermal storage capacity (melting enthalpy) of the coated material. Figure 3-13 shows the melting and freezing behavior of coated and uncoated material upon heating and cooling respectively. Heating and cooling rates were set to  $2\text{ }^{\circ}\text{C}\cdot\text{min}^{-1}$ . It can be seen that the melting point was not affected by the coating, but the storage capacity decreased.

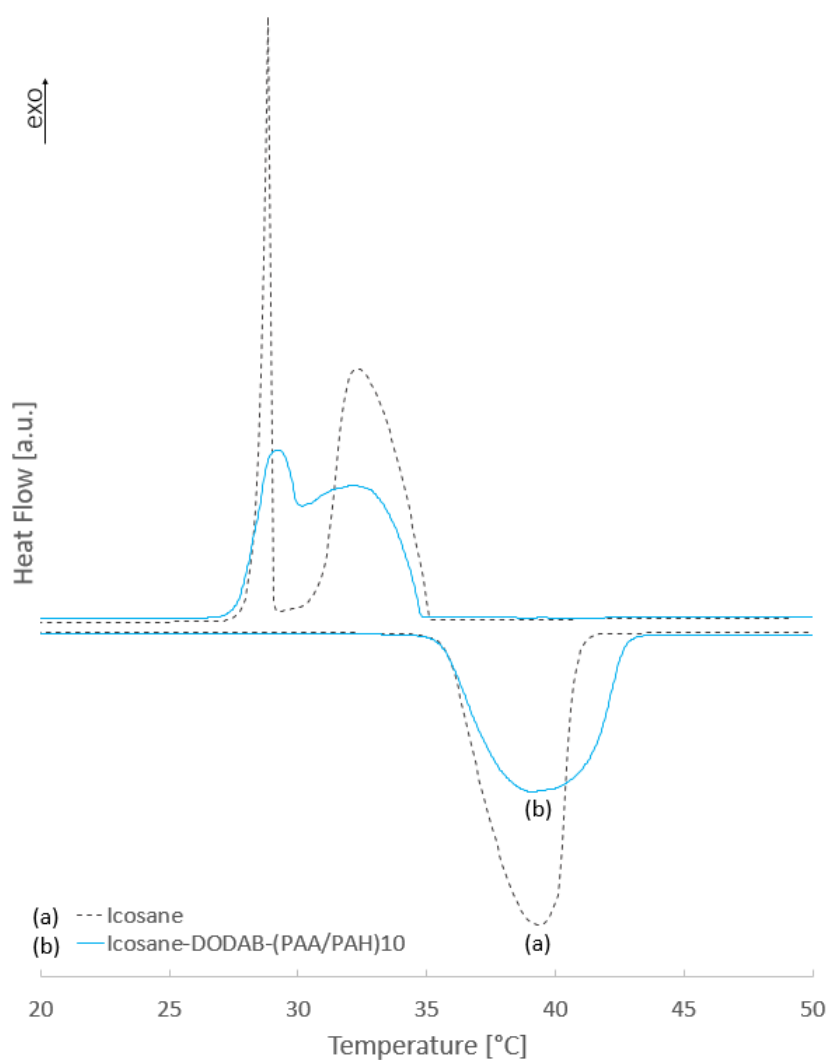


**Figure 3-13:** DSC traces of icosane (a) and Icosane-DODAB-(PAA/PAH)<sub>10</sub> (b) recorded at heating/cooling rate of  $2\text{ }^{\circ}\text{C}\cdot\text{min}^{-1}$ .

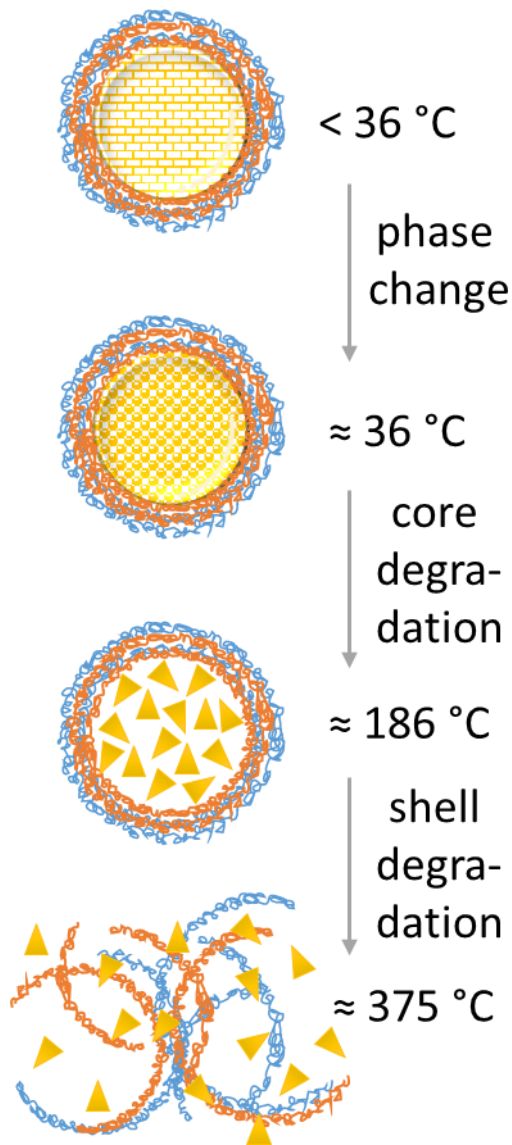


**Figure 3-14:** Schematic illustration of the TGA and DSC results.

As the shell material does not work as a storage material, naturally there is less storage capacity in 1 g of coated material than in 1 g of uncoated PCM. As mentioned in the introduction, the aim was to keep the storage capacity at a high value despite the reduction caused by the coating. Pristine icosane shows a melting enthalpy of  $223.6 \text{ J}\cdot\text{g}^{-1}$  (Figure 3-13a). Compared to that, the storage capacity of icosane-DODAB-(PAA/PAH)<sub>10</sub> is only moderately reduced, displaying a value of  $199.1 \text{ J}\cdot\text{g}^{-1}$  (Figure 3-13b). Similar to the summary of the thermal evaluation in chapter 2, the relation of the

DSC and TGA findings is displayed in Figure 3-14.

It can be seen the first thermal event during the heating process is the phase change of icosane around  $36\text{ }^\circ\text{C}$ . This is followed by the degradation of the core ( $T_{10} = 186.5\text{ }^\circ\text{C}$ ) and finally resulting in the destruction of the particles when the shell starts degrading (around  $375\text{ }^\circ\text{C}$ ). As a comparable and commercially available product like Rubitherm RT42 with a melting temperature of  $41\text{ }^\circ\text{C}$  shows a heat storage capacity of  $165 \text{ J}\cdot\text{g}^{-1}$ , the material is considered suitable for use in thermal energy storage applications.<sup>33</sup>

The PCM content of icosane-DODAB-(PAA/PAH)<sub>10</sub> was calculated using the melting and freezing enthalpies of coated and uncoated particles by the following equation (Equation 3-2):

$$PCM \text{ content} = \frac{\Delta h_{m,LbL} + \Delta h_{c,LbL}}{\Delta h_{m,icosane} + \Delta h_{c,icosane}} \times 100\% = 88.6 \%$$
 (Equation 3-2)

Where  $\Delta h_m$  and  $\Delta h_c$  denote the phase change enthalpy recorded during melting and freezing respectively and LbL and icosane indices declare the enthalpies belonging to the coated and uncoated PCM respectively. We found a PCM content of 89 % from our calculations, which is in good accordance with the findings from the TGA.

Additionally, the stability of icosane-DODAB-(PAA/PAH)<sub>10</sub> was evaluated by performing a short thermal cycling test including 100 consecutive heating and cooling operations (Figure 3-15). The coated particles showed repeatable and stable phase change behavior in the tested range. Heat uptake and release occurred at constant high values around an average of 192 J·g<sup>-1</sup>. Upon closer examination, a slight shift of the melting peak top to a higher temperature can be noticed. This is attributed to the higher heating rate compared to the initial thermal evaluation in Figure 3-13 as the onset temperature of the melting process does not change significantly (10 °C min<sup>-1</sup>, peak 42.8 °C, onset 36.4 °C compared to 2 °C min<sup>-1</sup>, peak 39.0 °C, onset 35.6 °C).

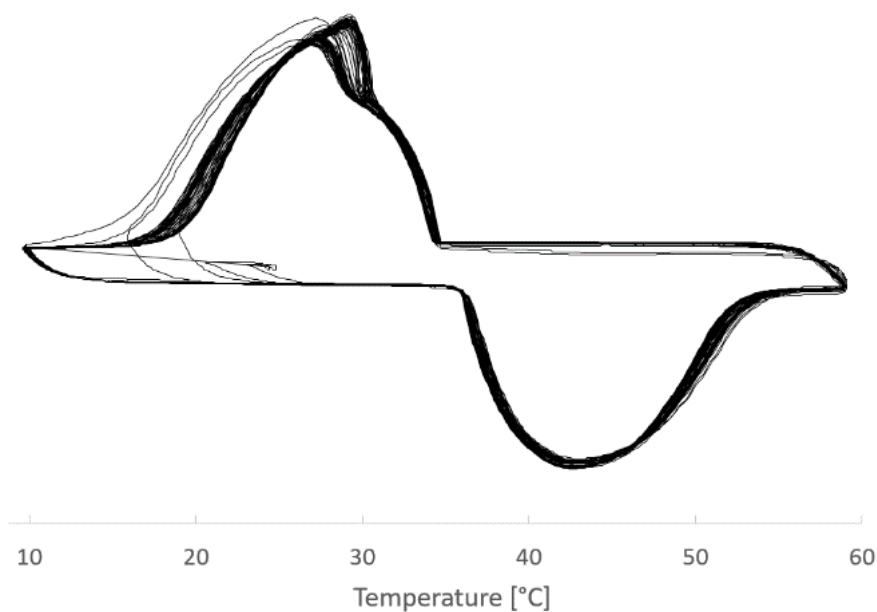


**Figure 3-15:** Multicycle DSC thermogram, heating and cooling rate  $10\text{ }^{\circ}\text{C min}^{-1}$ ,  $10\text{-}60\text{ }^{\circ}\text{C}$ .

It is expected that the particles can be properly used without significant performance losses for an increased number of heating-cooling circles as well.

No leakage of icosane was detected when the sample in the pan was evaluated by eye after 100 heating-cooling cycles in the DSC experiment; however, a comprehensive leakage test is necessary to evaluate the coating stability under working conditions. This is supposed to be part of a future work. Figure 3-16 shows a comparison of icosane-DODAB-(PAA/PAH)<sub>10</sub> before (Figure 3-16a) and after (Figure 3-16b) heating from  $10\text{ }^{\circ}\text{C}$  to  $60\text{ }^{\circ}\text{C}$  during 100 DSC cycles and icosane under the same conditions before (Figure 3-16c) and after (Figure 3-16d) during two DSC cycles. The coated particles were able to freely trickle out of the pan when it was turned upside down, indicating sufficient encapsulation ability of the applied coating. Free icosane melted completely, forming a wax-like coating on the bottom of the pan after cooling. For further evaluation of the coating stability, we heated the coated particles to  $130\text{ }^{\circ}\text{C}$  and

200 °C and kept them there for 1 h. After opening the pans, again, no obvious leakage could be detected, but the particles were sticking together, hinting at possible leakage of the PCM. Concluding from these results, the coated particles are stable in the desired temperature range around icosane's melting range but should not be exposed to excessive heat far outside the application window of the PCM.

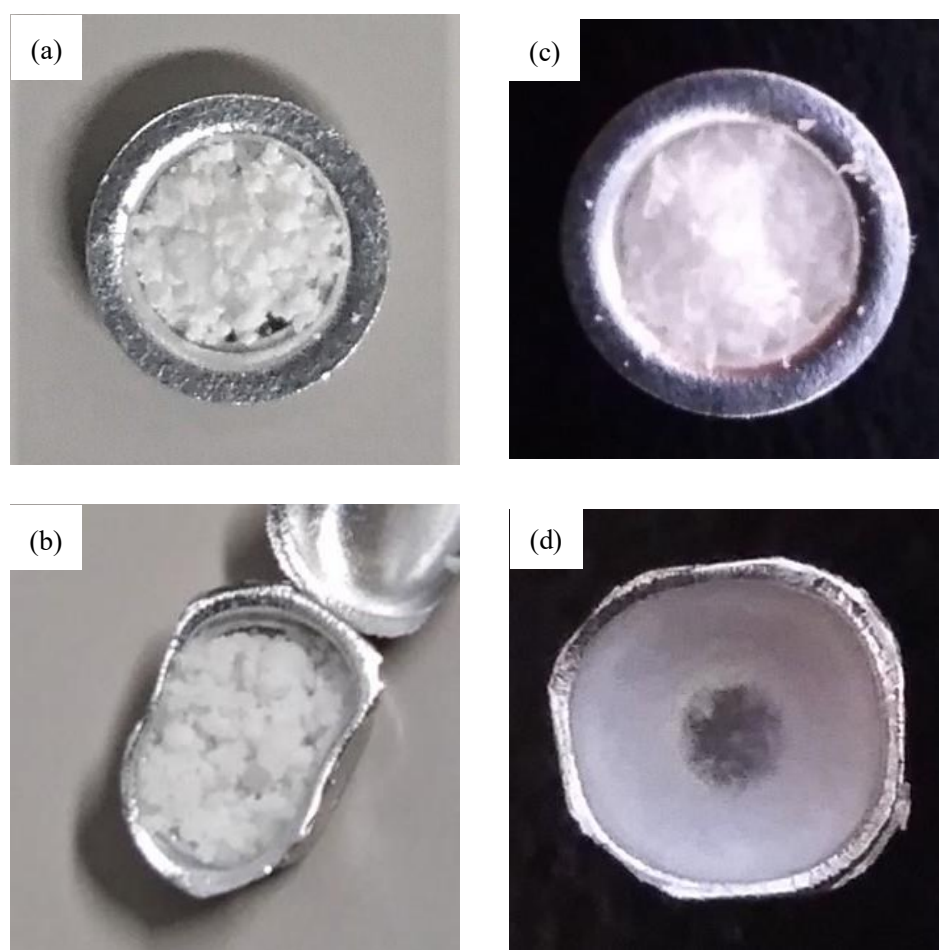


**Figure 3-16:** Comparison of icosane-DODAB-(PAA/PAH)<sub>10</sub> before (a) and after (b) 100 cycles of DSC measurements from 10 °C to 60 °C; similar conditions for icosane before (c) and after (d) two heating-cooling cycles.

FT-IR measurements (Figure 3-17) imply no changes in the chemical nature of the coated particles after 10 heating-cooling cycles (Figure 3-17b) and after heating and holding at 130 °C (Figure 3-17c).



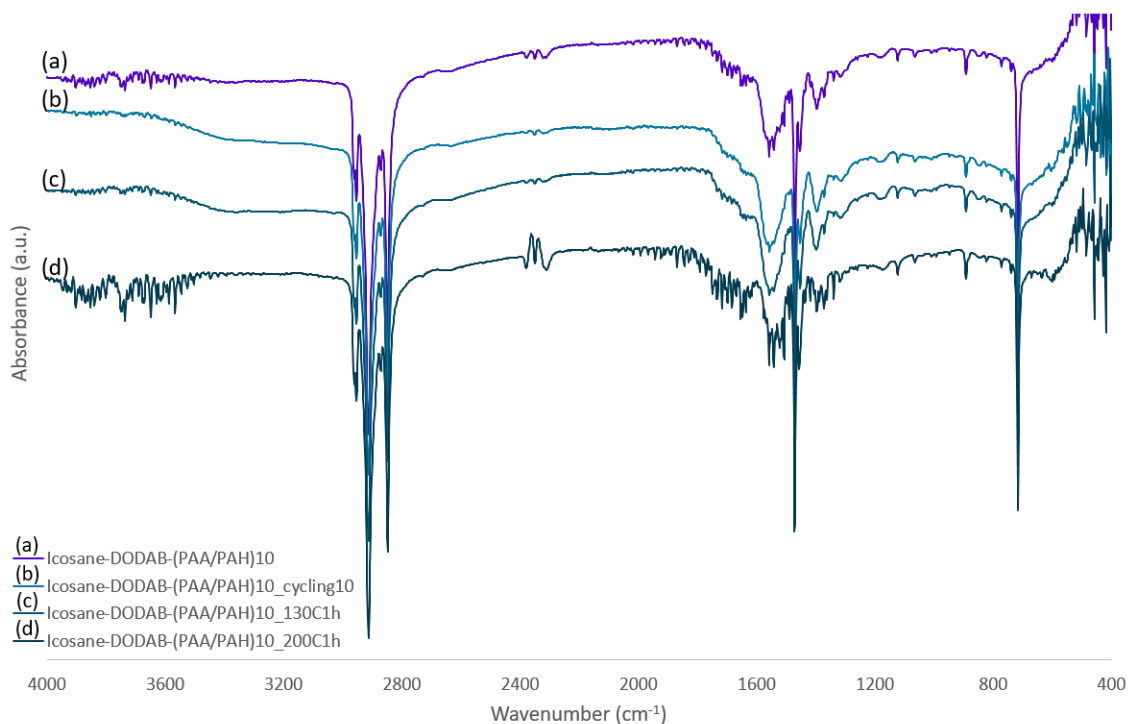


**Figure 3-17:** FT-IR spectra of coated particles after different heating processes.

It is assumed that the beginning degradation of the core material to be responsible for the noisy spectrum of the sample that was heated and held at 200 °C (Figure 3-17d). Related to this investigation, the possible formation of amide bonds between the coating layers, which would increase the robustness of our encapsulation by changing the electrostatic interaction to more stable covalent bonds was of high interest. Harris *et al.*<sup>22</sup> reported the formation of amide bonds between PAA and PAH upon heating to 130 °C and even an increased formation upon heating to 200 °C after deposition of nine bilayers. Contrary to their findings in FT-IR spectra, neither the disappearing of the carboxylate peaks at 1572  $\text{cm}^{-1}$  and 1399  $\text{cm}^{-1}$  nor the appearing of amide peaks at 1670  $\text{cm}^{-1}$  and 1540  $\text{cm}^{-1}$  could be confirmed after none of the heating steps. It would be interesting to enforce the amide formation for example by using an activator as it

might result in a better performance in terms of stability and robustness for cross-linked LbL coatings.

### 3.4 Conclusion

In conclusion, for the first time encapsulated icosane as a phase change material using a combination of weak polyelectrolytes in a self-assembled layer-by-layer coating were prepared. The ultra-thin coating from the LbL self-assembly provided a superior core-shell ratio of 88.6 %. Compared to bulk, the storage capacity of our material was only moderately reduced due to the encapsulation and is still showing sufficiently high values ( $\Delta h_{m, \text{icosane}} = 223.6 \text{ J}\cdot\text{g}^{-1}$  to  $\Delta h_{m, \text{capsule}} = 199.1 \text{ J}\cdot\text{g}^{-1}$ ) for thermal energy storage. The performance did not decrease after 100 consecutive heating-cooling cycles. The material displays improved thermal stability in the TGA tests ( $T_{10, \text{bulk}} = 175.7 \text{ }^\circ\text{C}$  and  $T_{10, \text{capsule}} = 186.8 \text{ }^\circ\text{C}$ ) and the encapsulation should enable it to be used in a broad range of possible applications. Moreover, the delayed thermal degradation of the coated material hints for a retardation effect provided by the coating. The homogenous particle size of about 20 to 50  $\mu\text{m}$  observed by SEM proved suitable for good heat conductivity throughout the whole particle to the core of the capsule. This approach is easily transferable to similar paraffin-type PCMs. Compared to chapter 2 the use of an emulsion for the particle preparation seems to have greatly facilitated the adsorption process. Due to the already spherical shape in solid state, the forces, which appear during the phase change, might have been reduced.

When the core turns liquid and adopts the drop-like shape, the shell materials do not need to rearrange very much. Thus, the coating is not ruptured during the phase change. Moreover, the additional layer provided by the surfactant is able to connect the core to the shell directly and is believed to support greatly the stability of the core-shell structure. Like this, the complementary approach presented in this chapter can provide a blueprint for other hydrophobic PCMs.

### 3.5 References

1. Pielichowska K.; Pielichowski K. Phase change materials for thermal energy storage. *Prog. Mater. Sci.* **2014**, *65*, 67-123.
2. Su W.; Darkwa J.; Kokogiannakis G. Review of solid-liquid phase change materials and their encapsulation technologies. *Renew. Sust. Energ. Rev.* **2015**, *48*, 373-391.
3. Tumirah K.; Mohd Z. H.; Zulkarnain Z.; Rafeadah R. Encapsulation techniques for organic phase change materials as thermal energy storage medium: A review. *Sol. Energ. Mater. Sol. C.* **2015**, *143*, 78-98.
4. Miliána Y. E.; Gutiérrez A.; Grágeda M.; Ushak S. A review on encapsulation techniques for inorganic phase change materials and the influence on their thermophysical properties. *Renew. Sust. Energ. Rev.* **2017**, *73*, 983-999.
5. Shchukina E. M.; Graham M.; Zheng Z.; Shchukin D. G. Nanoencapsulation of phase change materials for advanced thermal energy storage systems. *Chem. Soc. Rev.* **2018**, *47*, 4156-4175.
6. Ping L.; Wenshuai C.; Juanjuan F.; Rawan G.; Min Z.; Thermally Triggered Nanocapillary Encapsulation of Lauric Acid in Polystyrene Hollow Fibers for Efficient Thermal Energy Storage. *ACS Sustain. Chem. Eng.* **2018**, *6*, 2656-2666.
7. Xiao Z. Q.; Yuan T.; Xue Q. X.; Xin Q. X.; Xiao Y. F. Synthesis and characterization of paraffin/TiO<sub>2</sub>-P(MMA-co-BA) phase change material microcapsules for thermal energy

- storage. *J. Appl. Polym. Sci.* **2018**, *135*, 46447.
8. Mochane M. J.; Luyt A. S. Preparation and properties of polystyrene encapsulated paraffin wax as possible phase change material in a polypropylene matrix. *Thermochimica Acta.* **2016**, *544*, 63-70.
  9. Makuta T.; Kadoya K.; Izumi H.; Miyatake M. Synthesis of cyanoacrylate-covered xylitol microcapsules for thermal storage. *Chem. Eng. J.* **2015**, *273*, 192-196.
  10. Chaiyasat P.; Noppalit S.; Okubo M.; Chaiyasat A. Innovative synthesis of high performance poly(methyl methacrylate) microcapsules with encapsulated heat storage material by microsuspension iodine transfer polymerization (*ms* ITP). *Sol. Energ. Mater. Sol. C.* **2016**, *157*, 996-1003.
  11. Döğüşcü D. K.; Kizil Ç.; Biçer A.; Sari A.; Alkan C. Microencapsulated *n*-alkane eutectics in polystyrene for solar thermal applications. *Sol. Energy.* **2018**, *160*, 32-42.
  12. Hayashi Y.; Fuchigami K.; Taguchi Y.; Tanaka M. Preparation of microcapsules containing erythritol with interfacial polycondensation reaction by using the (w/o) emulsion. *J. Encap. Adsorp. Sci.* **2014**, *4*, 132-141.
  13. Rezvanpour M.; Hasanzadeh M.; Azizi D.; Rezvanpour A.; Alizadeh M. Synthesis and characterization of micro-nanoencapsulated *n*-eicosane with pmma shell as novel phase change materials for thermal energy storage. *Mater. Chem. Phys.* **2018**, *215*, 299-304.
  14. Zhu Y.; Chi Y.; Liang S.; Luo X.; Chen K.; Tian C.; Wang J.; Zhang L. Novel metal

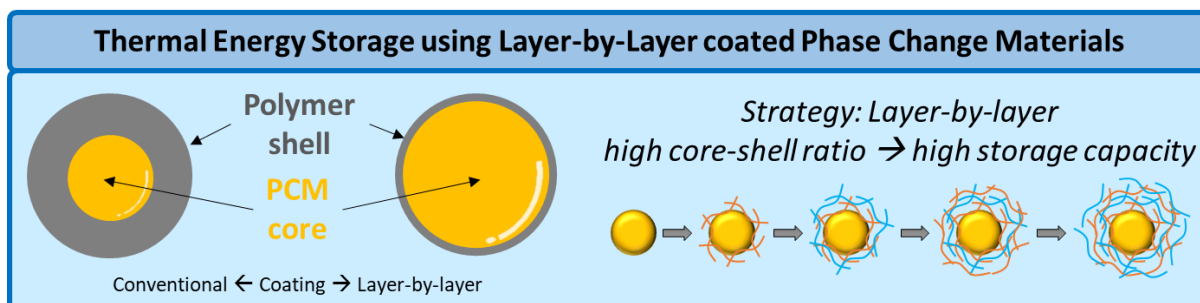
- coated nanoencapsulated phase change materials with high thermal conductivity for thermal energy storage. *Sol. Energ. Mater. Sol. C.* **2018**, *176*, 212-221.
15. Richardson J. J.; Cui J.; Björnmalm M.; Braunger J. A.; Ejima H.; Caruso F. Innovation in layer-by-layer assembly. *Chem. Rev.* **2016**, *116*(23), 14828-14867.
  16. Decher G. Fuzzy nanoassemblies: toward layered polymeric multicomposites. *Science.* **1997**, *277*, 1232-1237.
  17. Serizawa T.; Hamada K.; Kitayama T.; Fujimoto N.; Hatada K.; Akashi M. Stepwise stereocomplex assembly of stereoregular poly(methyl methacrylate)s on a substrate. *J. Am. Chem. Soc.* **2000**, *122*, 1891-1899.
  18. Matsusaki M.; Ajiro H.; Kida T.; Serizawa T.; Akashi M. Layer-by-layer assembly through weak interactions and their biomedical applications. *Adv. Mater.* **2012**, *24*, 454-474.
  19. Ajiro H.; Hinoue T.; Akashi M. Inkjet Approaches Contribute to Facile Isotactic Poly(Methyl) Syndiotactic Poly(Methyl Methacrylate) Stereocomplex Surface Preparations. *Macromol. Chem. Phys.* **2013**, *214*, 1590-1595.
  20. Seitz S.; Akashi M.; Ajiro H. Pentaerythritol particles covered by layer-by-layer self-assembled thin films with stereocomplex of isotactic poly(methyl methacrylate) and syndiotactic poly(methyl methacrylate). *Colloid Polym. Sci.* **2017**, *295*(155), 1541-1548.
  21. Shiratori S. S.; Rubner M. F. pH-dependent behavior of sequentially adsorbed layers of

- weak polyelectrolytes. *Macromolecules*. **2000**, *33*, 4213-4219.
22. Harris J. J.; DeRose P. M.; Breuning M. L. Synthesis of passivating, nylon-like coatings through cross-linking of ultrathin polyelectrolyte films. *J. Am. Chem. Soc.* **1999**, *121*, 1978-1979.
23. Zhao J.; Yang Y.; Li Y.; Zhao L.; Wang H.; Song G.; Tang G. Microencapsulated phase change materials with TiO<sub>2</sub>-doped PMMA shell for thermal energy storage and UV-shielding. *Sol. Energ. Mater. Sol. C.* **2017**, *168*, 62-68.
24. Lashgari S.; Mahdavian A. L.; Arabi H.; Ambrogi V.; Marturano V. Preparation of acrylic PCM microcapsules with dual responsivity to temperature and magnetic field changes. *Eur. Polym. J.* **2018**, *101*, 18-28.
25. Gao F.; Wang X.; Wu D.; Design and fabrication of bifunctional microcapsules for solar thermal energy storage and solar photocatalysis by encapsulating paraffin phase change material into cuprous oxide. *Sol. Energ. Mater. Sol. C.* **2017**, *168*, 146-164.
26. Iamphaojeen Y.; Siriphannon P. Adjustable thermal barrier of cotton fabric by multilayer immobilization of PCM nanocapsules. *Cellulose*. **2018**, *25*(6), 3649-3661.
27. Gondora W.; Doudin K.; Nowakowski D. J.; Xiao B.; Ding Y. L.; Bridgewater T.; Yuan Q. C. Encapsulation of phase change materials using rice-husk-char. *Appl. Energ.* **2016**, *182*, 274-281
28. Yi Q. Y.; Sukhorokov G. B.; Ma J.; Yang X. B.; Gu Z. W.; Encapsulation of phase change

- materials using layer-by-layer assembled polyelectrolytes. *Int. J. Polym. Sci.* **2015**, article number: 756237, doi: 10.1155/2015/756237
29. Alkilani M. M.; Sopian K.; Alghoul M. A.; Sohif M.; Ruslan M. H. Review of solar air collectors with thermal storage units. *Renew. Sust. Energ. Rev.* **2011**, *15*, 1476-1490.
  30. Grigoriev D. O.; Bukreeva T.; Möhwald H.; Shchukin D. G.; New method for fabrication of loaded micro- and nanocontainers: emulsion encapsulation by polyelectrolyte layer-by-layer deposition on the liquid core. *Langmuir.* **2008**, *24*, 999-1004.
  31. Sauerbrey G. Verwendung von Schwingquarzen zur Wägung dünner Schichten und zur Mikrowägung. *Z. Phys.* **1959**, *155*, 206-222.
  32. Bieker P.; Schönhoff M. Linear and Exponential Growth Regimes of Multilayers of Weak Polyelectrolytes in Dependence on pH. *Macromolecules.* **2010**, *43*, 5052-5059.
  33. Borges J.; Mano J.F. Molecular Interactions Driving the Layer-by-Layer Assembly of Multilayers. *Chem. Rev.* **2014**, *114*, 8883-8942.
  34. Rubitherm RT42, Product Data Sheet, Rubitherm Technologies GmbH, Sperenberger Str. 5a, D-12277 Berlin



## CONCLUDING REMARKS



The scope of this dissertation is the preparation of Layer-by-Layer coated phase change materials as thermal energy storage materials. In the larger view, these applications can be part of the solution of the global challenges concerning the energy supply and utilization of green energy technologies. The LbL approach is chosen in this work because of its flexible design and straightforward, easy to adjust preparation, but especially because of its ability to produce ultra-thin layers, which are beneficial to the core-shell ratio and therefore enable so prepared materials for storage capacities close to the pristine PCMs. The corresponding core materials are selected carefully and represent a different material class in each chapter. The results obtained through this work are summarized as follows.

### Chapter 1

#### Background: Thermal Energy Storage & Encapsulation of PCM

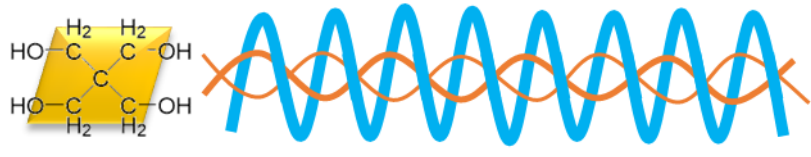
Chapter 1 is presenting the broad picture of thermal energy storage in the beginning. Several PCMs are described and grouped according to their chemical nature. Next, the advantages of encapsulated PCMs are pointed out and various encapsulation methods are

depicted. It is understood that the particles size is strongly corresponding to the heat transfer area available for the process and thus plays a vital role in the storage and release processes. Another important point to consider is how the heat is actually transported from one system to another. Several specific designs for heat exchangers are available to make even more use of PCMs' storage abilities. These, however, are out of the scope of this thesis. Finally, the importance of the core-shell ratio is pointed out. This ratio is a main factor in achieving suitable storage capacities for industrial and domestic or building applications. The introduction part also picks up the importance of the core-shell ratios as well as encapsulated PCMs. An approach based on LbL self-assemblies is pointed out as a high potential encapsulation approach. Due to the nature of LbL films to be arranged in the nanometer order, they appear extremely interesting as coatings for PCMs. Stereoregular isotactic and syndiotactic PMMA assembled as a stereocomplex coating as well as electrostatic interacting poly(acrylic acid) and poly(allyl amine) are proposed as promising coating materials for hydrophilic and hydrophobic cores respectively. These materials are then introduced in the following chapters.

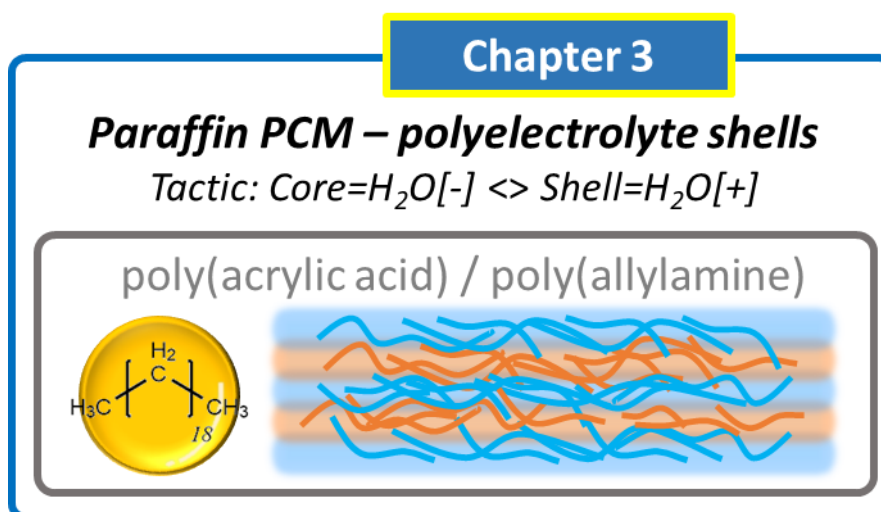
**Chapter 2**

***Sugar alcohol PCM – stereoregular shells***  
*Tactic: Core=H<sub>2</sub>O[+] <> Shell=H<sub>2</sub>O[-]*

(isotactic) *it*- / (syndiotactic) *st*-PMMA



In chapter 2, LbL coated pentaerythritol particles are described. Isotactic and syndiotactic PMMA were used as coating materials. The performed experiments were used to make a general statement about the stereocomplex LbL coating on a sugar alcohol PCM substrate. In relation to this, stepwise and steady growth of the shell thickness was confirmed by QCM measurements. The successful coating was finally evaluated by FT-IR. DSC and TGA revealed the good compatibility of the core and shell materials in terms of thermal properties and proved that the herein presented concept is suitable for the preparation of PMMA-stereocomplex coated pentaerythritol PCM particles.



In chapter 3, LbL coated icosane particles are presented. The shell layers are a combination of poly(acrylic acid) and poly(allyl amine) and the stepwise layer adsorption was demonstrated using QCM. With this material combination, novel PCMs with a high core-shell ration of about 90 % have been prepared. The successful coating was confirmed by FT-IR, <sup>1</sup>H NMR, TGA and microscopy including fluorescence microscopy. With this elegant coating method, storage capacities of the coated materials close to the pristine icosane were achieved

and confirmed by DSC. Moreover, cycling stability was confirmed for more than 100 heating-cooling cycles. Target application of such materials could be found as a PCM in solar air collectors equipped with thermal storage units. A comparison with the only other report in the field of LbL coated PCMs for TES (ow: own work, Ref 1: see chapter 3, ref 28) revealed the good properties of the developed storage material (Table 4-1, Figure 4-1).

**Table 4-1:** Comparison of the current approach and an example from literature (ow: own work, Ref 1: Yi et al. *Int. J. Polym. Sci.* **2015**, article number: 756237, doi: 10.1155/2015/756237).

Shell on C <sub>20</sub> core	T <sub>m</sub> (°C)	H <sub>m</sub> (J/g)	E (%)	Preparation	Ref
C <sub>20</sub> (icosane, C <sub>20</sub> H <sub>42</sub> )	35.7	223	/	Pristine PCM	ow
Icosane(PAA/PAH) <sub>10</sub>	36.5	191	85.5	Self-assembly	ow
C <sub>18</sub> (octadecane, C <sub>18</sub> H <sub>38</sub> )	31.3	189	/	Pristine PCM	1
Octadecane (PSS/PDADMAC) <sub>3</sub>	34.2	173	91.5	Self-Assembly	1

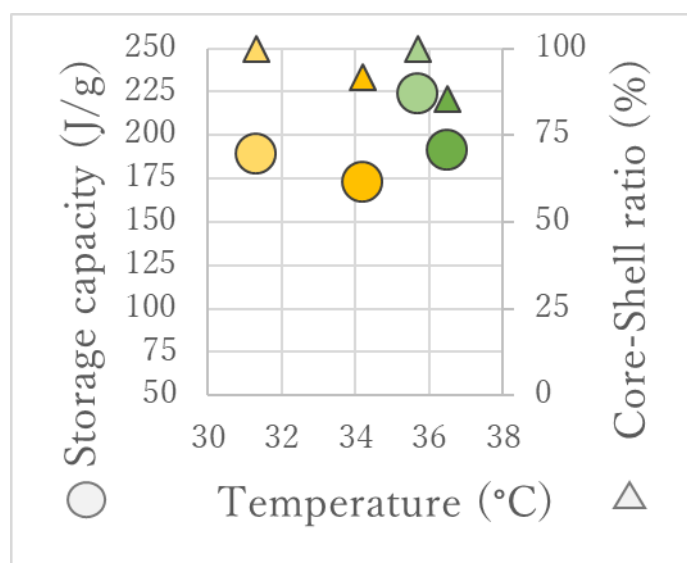


**Figure 4-1:** Visualization of the comparison from table 4-1.

With the yellow markers presenting the literature material, it can be seen that both

approaches can provide high thermal energy storage capacities. The material prepared in chapter 3 of this thesis shows an advantageous behavior when the shift of the melting temperature after coating is considered. That means that the melting temperatures of the pristine icosane and the coated particles are only deferring by less than 1 °C, which is very important to achieve predictable results for specific applications. The reduction of the storage capacity is about 6 % larger in the herein presented material. This is the result of the higher amount of coating material applied to the core particles. Nevertheless, due to the higher storage capacity of the pristine icosane compared to the pristine octadecane, the herein presented material can provide about 18 J g<sup>-1</sup> higher storage capacities.

Overall, this dissertation displays the impressive versatility of the Layer-by-Layer approach for the creation of environmental materials. The developed core-shell structures are exhaustively analyzed and evaluated. Suitable applications are presented in the corresponding chapters and the competitive performance of the prepared materials towards commercial products is pointed out. Moreover, the experimental procedures and processes had been improved throughout this thesis based on the previously achieved results in each chapter. Like this, all findings presented here can be considered important steps on the way to the finally reported materials.

As far as an outlook for future developments on the herein presented materials is concerned, several improvements could be pursued. On the one hand, the polymer chains in the

PMMA stereocomplex coatings could be chemically modified to obtain cross-linkable derivatives. An interesting approach on this has already been proposed by Vidal and coworkers (Vidal *et al.*, *J. Am. Chem. Soc.* **2016**, *138*, 9533-9547). It would be interesting to convey this concept for the application in LbL coatings for PCMs. On the other hand, the improvement of the encapsulation efficiency and an increased robustness for the polyelectrolyte coatings for paraffin-like PCMs would be of great interest as well. One approach to create such materials is the thermal cross-linking for the amid bond formation between PAA and PAH as already mentioned in this thesis. Another approach could be the introduction of a cross-linking small molecule, for example in the form of glutaraldehyde, which has already been shown to improve the mechanical and chemical properties of poly(ethylene imine)-PAA multilayers (Lindén, J.B. *et al. J. Appl. Polym. Sci.* **2016**, DOI: 10.1002/APP.43954.). Both approaches could be suitable to create more robust coatings, allowing for the reduction of the layer number and thus providing better core-shell ratios at the same time. This will ultimately yield higher storage capacities for the so prepared materials.

Many technical details of thermal energy storage were discussed throughout this thesis and the great potential of phase change materials was laid out. In the introduction, the assumption was made that PCMs could contribute significantly to answer the energy challenge. A strong hint that this is true is not only the technological potential, which is acknowledged in many papers and scientific publication, but also the predicted economic impact as pointed out

in numerous market analyses. The market size for advanced PCMs is will more than triple in less than ten years and reach a volume of 3.75 billion USD by 2026 (Reports and Data, Report ID RND\_001264, published April **2019**, Reports and Data, 40 Wall St. 28th floor New York City, NY 10005 United States). There is a big role for the PCM technology and thermal energy storage to play in the future.

Finally yet importantly, hopes are that the herein presented materials can inspire novel approaches to tackle the global challenges that humanity is facing and to support the change to a better world for future generations.

## LIST OF PUBLICATIONS

- 1) Steffen Seitz, Mitsuru Akashi, Hiroharu Ajiro.

Pentaerythritol Particles Covered by Layer-by-Layer Self Assembled Thin Films with Stereocomplex of isotactic Poly(methyl methacrylate) and syndiotactic Poly(methyl methacrylate).

*Colloid Polym. Sci.* **2017**, *295*, 1541-1548.

- 2) Steffen Seitz, Hiroharu Ajiro.

Self-Assembling Weak Polyelectrolytes for the Layer-by-Layer Encapsulation of Paraffin-Type Phase Change Material Icosane.

*Sol. Energy Mater. Sol. Cells.* **2019**, *190*, 57-64.

### Other Publications

- 1) Steffen Seitz, Hiroharu Ajiro.

Novel copper scavenging materials and facile recovery using poly(ethylene imine) based Layer-by-Layer coatings on icosane particles.

*in preparation.*

- 2) Soma Chakraborty, James Nicolas M. Pagaduan, Zarah Melgar, Steffen Seitz, Kai Kan,



Hiroharu Ajiro.

Glycerol-Modified Poly( $\epsilon$ -caprolactone): A Biocatalytic Approach to Improve The  
Hydrophilicity of Poly( $\epsilon$ -caprolactone)

*Polym. Bull.* **2019**, 76(4), 1915–1928.

## ACKNOWLEDGEMENTS

I would like to express my deep and heartfelt gratitude to my supervisor Professor Hiroharu Ajiro. I am grateful for his patient guidance and warm encouragement. His constructive critiques and his will to give his time so generously for teaching and advising are highly appreciated. He provided me with the opportunity and the freedom to learn and grow as a person. I will carry the knowledge and wisdom he shared with me wherever I go.

I would like to give my grateful thanks to my co-supervisors Professor Hisao Yanagi, Professor Yoichiroh Hosokawa, Assistant Professor Yoshiyuki Nonoguchi. Their advice helped me broaden my understanding about my topic and research in general. The valuable comments that I received during our discussions enabled me to improve a lot.

Professor Kiyomi Kakiuchi, Professor Pfeifer-Fukumura, and again to Professor Hisao Yanagi, and Prof Hiroharu Ajiro – I am deeply indebted to all of them. Their work and efforts made it possible for me to come to Japan and pursue this degree in the first place.

I would also like to thank NAIST technicians and staff for helping me during my work and stay and NAIST institutions for the financial support and chances, I received. I thank the

members of my laboratory, especially the first and former members for the warm welcome and teaching. A very special thank you is reserved for Nim for her kindness and cheerful support.

Finally, I would like to thank my love and my family in the simplest but most meaningful way as no words are sufficient for what I received from them: Thank you.